Table of Contents

List of Figures

CHAPTER 2: STATE OF THE ART

2.1 Overview of Crystal Engineering

2.1.1 Definition and Key Principles

Crystal engineering is a multidisciplinary field that focuses on the design, synthesis, and manipulation of crystalline materials with tailored properties, particularly by understanding and controlling intermolecular interactions such as hydrogen bonding, π–π stacking, van der Waals forces, and ionic interactions [40]. This field emphasizes the deliberate assembly of molecular building blocks into organized structures, aiming to achieve functional materials for various applications, including nonlinear optics [7]. At its core, crystal engineering involves the design of molecular components that assemble in a predictable and controlled manner, resulting in a crystalline material that exhibits the desired optical, mechanical, and electronic properties [32].

Key principles of crystal engineering include molecular design, supramolecular chemistry, polymorphism control, and defect engineering. Molecular design involves selecting or modifying molecules to create specific interactions that guide the assembly into ordered structures. Supramolecular chemistry refers to the use of non-covalent interactions to facilitate the self-assembly of molecules into crystals. Polymorphism control allows the formation of different crystal forms (polymorphs) of the same compound, each with distinct physical and chemical properties. Defect engineering is used to control the presence or absence of defects within crystals, which can influence their electronic and optical behavior [37].

In nonlinear optics, crystal engineering plays a critical role in creating materials with specific second-order nonlinear optical properties. A lack of a centrosymmetric structure is essential for nonlinear optical activity, and crystal engineering techniques have been used to design and synthesize materials like potassium titanyl phosphate (KTP) and lithium niobate ($LiNbO_3$), which possess non-centrosymmetric crystal structures necessary for efficient second-harmonic generation (SHG) [32].

2.1.2 Historical Development in Crystal Engineering

The concept of crystal engineering traces back to early theoretical work in the 20th century, but it gained practical significance in the 1980s, particularly through the pioneering contributions of Desiraju. His work on the role of non-covalent interactions in crystal formation established the foundations of modern crystal engineering. Desiraju's approach highlighted how intermolecular forces such as hydrogen bonding could be manipulated to control the arrangement of molecules in the solid state, laying the groundwork for the systematic design of functional crystalline materials [7].

In the field of nonlinear optics, crystal engineering emerged as a response to the growing demand for materials capable of efficient frequency conversion in lasers and photonics. The synthesis of nonlinear optical materials with tailored properties became crucial in the mid-20th century, particularly after the advent of high-power lasers. Early breakthroughs such as the development of KTP and $LiNbO_3$ crystals were instrumental in enabling practical applications such as optical parametric oscillators (OPOs), which rely on the efficient conversion of light into new wavelengths through SHG [38].

In recent years, there has been a significant shift toward the design of organic and hybrid materials for nonlinear optics. Organic materials, due to their ease of synthesis and tunable properties, have attracted increasing interest for applications in photonics. The design of organic nonlinear optical materials involves selecting molecules with large dipole moments and polarizabilities, arranging them in non-centrosymmetric crystal lattices to achieve desired nonlinear optical properties. The development of organic crystals such as 2-methyl-4-nitroaniline (MNA) has demonstrated the potential for these materials to outperform traditional inorganic crystals in certain applications [32]. These materials provide the advantage of ease in processing and tunable properties, making them attractive for use in integrated photonics and other emerging technologies.

Thus, crystal engineering has evolved significantly from its early theoretical roots, and its applications have expanded to include the design of advanced materials for nonlinear optical devices. This shift toward functional crystal design has not only enhanced the performance of

existing optical devices but also opened up new avenues for the development of next-generation photonic technologies [7].

2.2 Nonlinear Optical Materials

2.2.1 Introduction to Nonlinear Optics

Nonlinear optics (NLO) encompasses the study of optical phenomena that occur when the response of a material to an electromagnetic field is nonlinear, meaning the polarization P does not respond linearly to the electric field E. This nonlinearity becomes significant at high light intensities, leading to phenomena such as second-harmonic genera tion (SHG), third-harmonic generation (THG), and optical rectification. These effects are pivotal in the development of advanced photonic devices, including frequency converters, optical switches, and modulators [3].

Second-order nonlinear optical materials are particularly crucial for SHG, where two photons combine to form a new photon with twice the energy and half the wavelength of the original photons. For efficient SHG, the material must lack a center of symmetry, a property known as acentrosymmetry. Materials exhibiting this symmetry are essential for generating coherent light at new wavelengths, enabling applications in laser sources, telecommunications, and medical diagnostics [39].

2.2.2 2-Methyl-4-Nitroaniline (MNA) as a Nonlinear Optical Material

2-Methyl-4-nitroaniline (MNA), with the chemical formula $C_7H_8N_2O_2$, is an organic compound that has garnered significant attention for its nonlinear optical properties. The molecular structure of MNA features an electron-donating methyl group at the para position and an electron-withdrawing nitro group at the meta-position relative to the amino group on the benzene ring. This arrangement creates a large dipole moment, essential for nonlinear optical activity [18].

The acentrosymmetric nature of MNA crystals is a key factor in their nonlinear optical behavior. Studies have demonstrated that MNA crystals crystallize in non-centrosymmetric space groups, making them suitable candidates for SHG applications [46]. The large dipole moment and the ability to form non-centrosymmetric crystals contribute to MNA's significant second-order

nonlinear optical coefficients, making it an attractive material for frequency conversion processes.

Optical characterization of MNA has revealed impressive nonlinear optical properties. For instance, MNA exhibits a large second-order susceptibility ($\chi(2)$), which is a measure of its efficiency in generating second-harmonic light. This high $\chi(2)$ value indicates that MNA can efficiently convert incident light to its second harmonic, a desirable trait for various photonic applications [26].

The applications of MNA in photonic systems are diverse. Its high nonlinear optical coefficients make it suitable for use in optical parametric oscillators (OPOs), which are devices that generate tunable coherent light by mixing two photons of different frequencies. Additionally, MNA's properties are beneficial in the development of electro-optic modulators and optical switches, which are integral components in telecommunications and information processing systems [3].

In summary, MNA's molecular structure, acentrosymmetric crystallization, and substantial nonlinear optical coefficients position it as a promising material for various photonic applications. Its role in advancing nonlinear optical technologies underscores the importance of organic materials in the development of next-generation photonic devices.

2.3 Nanoconfinement in Crystal Growth

2.3.1 Effects of Confinement on Crystal Growth

Nanoconfinement significantly influences the crystallization process, particularly within nanopores, by altering nucleation rates, crystal size, and morphology. The spatial constraints imposed by nanopores restrict the movement of molecules, leading to changes in the crystallization dynamics.

In confined environments, nucleation often becomes localized near the edges of the pores due to concentration gradients and limited diffusion pathways. For instance, in studies of $NaClO_3$ crystals growing in nanoconfinement, nucleation events were predominantly observed at the contact edges, with minimal activity at the center of the confined space [21]. This localization is

attributed to the depletion of ions near the growing crystal surface, which hinders diffusion and favors edge nucleation.

The size and morphology of crystals are also affected by confinement. In nanopores, crystals often exhibit reduced dimensions and altered shapes compared to their bulk counterparts. For example, when polymers are confined within rigid nanoporous anodic aluminum oxide (AAO) templates, their crystallization behavior experiences dramatic changes, such as fractionated crystallization and exclusive crystallization at much higher supercoolings compared to bulk polymers [28]. This indicates that confinement can induce polymorphism and influence the crystalline phase formed.

Additionally, confinement can lead to the formation of unique crystal morphologies. In the case of $NaClO_3$ crystals, confined growth resulted in the development of skewed dislocation spirals and kinetic localization of nucleation near the contact edge, leading to distinctive growth patterns [21]. Such behaviors are governed by the two-dimensional transport of mass through the liquid film from the edges to the center of the contact, which produces gradients that control the growth of new molecular layers.

2.3.2 Models of Nanoconfinement

To study the effects of confinement on crystal growth, various models have been developed, with AAO templates being a prominent example. AAO templates consist of highly ordered nanopores that can be precisely controlled in terms of size and spacing, making them ideal for investigating nanoconfined crystallization.

Research has shown that when polymers are confined within AAO templates, the nanoconfinement effect induces a preferential crystal orientation, increasing the crystallization temperature and altering the crystalline phase compared to bulk materials [2]. This demonstrates the utility of AAO templates in controlling the crystallization process and achieving desired material properties.

Furthermore, AAO templates have been used to study the crystallization behavior of various compounds, including organic and inorganic materials. For instance, the crystallization of 3-

pentadecylphenol (PDP) within AAO templates was investigated to understand the melting and crystallization behaviors under nanoconfinement [25]. Such studies provide insights into how confinement affects the phase transitions and stability of materials.

In summary, nanoconfinement within AAO templates offers a controlled environment to study and manipulate crystal growth. The confinement effects lead to localized nucleation, altered crystal sizes and morphologies, and the formation of unique growth patterns. These findings underscore the importance of confinement in tailoring the properties of crystalline materials for various applications.

2.4 Crystallization Techniques

2.4.1 Methods of Crystallization

Crystallization techniques are essential in controlling the structural properties of organic nonlinear optical (NLO) materials, which directly impact their efficiency in photonic applications. Several methods, such as sublimation, melt infiltration, solution infiltration, and vapor deposition, are employed to form high-quality crystals with tailored properties [8].

Sublimation involves the direct phase transition of a material from a solid to a gas, followed by condensation. This method is particularly useful for purifying organic NLO materials and achieving highly crystalline structures. For instance, sublimation has been used to produce high-quality crystals of organic nonlinear optical materials like MNA (2-methyl-4-nitroaniline), which exhibit excellent electro-optic properties [5]. The sublimation process allows the controlled formation of polymorphs, which can have significant implications for enhancing the nonlinear optical response [34].

Melt Infiltration is another technique where a molten material is introduced into a porous substrate, where it solidifies upon cooling. This method is especially effective when working with photonic crystals, allowing for the formation of functional materials with controlled geometries and enhanced optical properties. For example, in one study, melt infiltration was used to integrate organic NLO materials into photonic crystal structures, achieving highly ordered and efficient devices [25].

Solution Infiltration involves dissolving the material in a solvent, which is then introduced into a porous template. After the solvent evaporates, the material crystallizes within the pores. This technique has been widely used for infiltrating photonic crystals with organic materials to enhance their nonlinear optical properties. For instance, solution infiltration of MNA in self-ordered anodic aluminum oxide (AAO) templates has been demonstrated to significantly improve crystal alignment and nonlinear optical behavior [47].

Vapor Deposition includes methods like physical vapor deposition (PVD), where material vapor condenses on a substrate to form a thin film. This technique is commonly used for creating organic NLO films with controlled thickness and uniformity. Vapor deposition of materials such as MNA has been used to produce films with excellent nonlinear optical coefficients, which are crucial for devices like optical switches and modulators [1].

Each of these techniques has its own advantages depending on the desired material properties. The choice of method affects crystal size, morphology, and the alignment of chromophores, which in turn influences the efficiency of second-order nonlinear optical processes like second-harmonic generation (SHG).

2.4.2 Techniques for Studying Crystallization

To understand the crystallization process and the properties of the resulting crystals, various characterization techniques are employed. These methods help in evaluating crystal quality, structure, and orientation, which are critical for optimizing nonlinear optical properties.

X-ray Diffraction (XRD) is one of the most widely used techniques to study crystal structure, unit cell dimensions, and symmetry. Single-crystal XRD provides precise data on atomic positions and bonding, which is essential for understanding the molecular packing within the crystal lattice. This technique is invaluable for investigating the crystallization of organic NLO materials, as it helps identify the non-centrosymmetric structures required for efficient nonlinear optical performance [1].

Scanning Electron Microscopy (SEM) allows high-resolution imaging of crystal surfaces, revealing information about crystal morphology, surface defects, and grain boundaries. SEM is

particularly useful for studying the surface features of organic NLO crystals, as it provides insights into their growth mechanisms and the factors influencing their optical properties. For instance, SEM analysis of MNA crystals grown in nanopores has shown how confinement affects the crystal size and orientation [47].

Thermal Analysis, including Differential Scanning Calorimetry (DSC), assesses the thermal behavior of crystals, including melting points, crystallization temperatures, and phase transitions. These techniques are crucial for understanding the stability and thermal properties of NLO materials. DSC has been used to study the crystallization and melting behavior of organic NLO materials like MNA, helping to optimize the crystallization conditions for better device performance [14].

In addition to these techniques, understanding the crystallographic texture and orientation is crucial for optimizing the nonlinear optical properties of materials. The alignment of chromophores within the crystal lattice directly affects the efficiency of second-order nonlinear optical processes, such as SHG and electro-optic modulation. Therefore, using XRD and SEM to assess and control crystal orientation during crystallization is critical for achieving high-performance NLO devices [1].

2.5 State of the Art in MNA Crystallization in Nanopores

2.5.1 Previous Studies on MNA Crystallization

Research on the crystallization of 2-methyl-4-nitroaniline (MNA) within confined geometries, particularly nanopores, is limited. However, studies on related compounds provide insights into how confinement influences crystallization. For instance, the crystallization behavior of ionic liquids in nanopores has been extensively studied. He et al. (2025) observed that the crystallization of imidazolium ionic liquids in nanopores was influenced by pore size and surface modifications, leading to changes in melting points and crystalline phases. These findings suggest that similar effects could be expected for MNA, where confinement could alter nucleation rates and crystal morphology.

Surface modifications of nanopores have also been shown to impact crystallization. In the study by He et al. (2025), tethering ionic liquids to pore walls promoted crystallization and stabilized specific crystal phases. Applying similar surface modification strategies to MNA could potentially enhance its crystallization behavior within nanopores.

2.5.2 Limitations and Gaps in Existing Research

Despite the valuable insights from related studies, there are significant gaps in understanding the crystallization of MNA within nanopores. The specific effects of pore size, geometry, and surface modifications on MNA crystallization remain unexplored. Additionally, the influence of confinement on the nonlinear optical properties of MNA crystals has not been investigated. Addressing these gaps is crucial for tailoring MNA crystals for advanced photonic applications.

Furthermore, existing studies often focus on bulk crystallization behaviors, with limited attention to the nanoscale effects that are critical in confined environments. There is a need for research that bridges this gap by examining MNA crystallization at the nanoscale, considering factors such as molecular interactions, nucleation kinetics, and crystal growth mechanisms within nanopores.

Overall, while there is a foundation of knowledge regarding crystallization in confined geometries, specific research on MNA crystallization within nanopores is lacking. Future studies should aim to fill these gaps by exploring the nanoscale crystallization behavior of MNA, the impact of confinement on its nonlinear optical properties, and the role of surface modifications in controlling crystal growth.

CHAPTER 3: METHODS AND MATERIALS

3.1 Experimental Methods

This section outlines the experimental techniques employed to study the crystallization behavior, morphology, and optical properties of MNA (2-methyl-4-nitroaniline) crystals, especially under confinement within nanopores.

3.1.1 X-ray Diffraction (XRD) for Crystallization Analysis of MNA Crystals

X-ray diffraction (XRD) is a cornerstone analytical technique for investigating the crystallization behavior and orientation of materials at the atomic level, particularly useful for materials like **2-Methyl-4-Nitroaniline (MNA)**, which is essential in nonlinear optical applications. This technique utilizes X-rays to probe the periodic structure of crystalline substances. The diffraction pattern provides direct insights into the crystal lattice's periodicity, orientation, and phase structure [11]. A PANalytical X'Pert Pro MRD X-ray diffractometer, which employs **Cu-Kα radiation** (wavelength λ=1.541 A˚), is used to analyze MNA crystals. The use of Cu-Kα radiation is standard in XRD studies due to its appropriate energy levels for most crystalline materials, ensuring effective interaction with the electron cloud of atoms within the crystal lattice [1].

The technique involves positioning the MNA sample on an **Eulerian cradle**, which is capable of rotating about three axes, enabling diffraction data to be captured from multiple orientations. This orientation flexibility is pivotal for studying the crystallographic phase, lattice spacing, and orientation of MNA crystals confined within **anodic aluminum oxide (AAO)** nanopores. The primary outputs from XRD studies include diffraction peaks, which, when analyzed, reveal key structural parameters such as lattice constants, crystal symmetry, and domain sizes [45].

Two fundamental XRD techniques employed in this analysis are **θ-2θ scans** and **Schulz scans**:

1. **θ-2θ Scans**:
   This technique measures the intensity of diffracted X-rays as a function of the incident angle θ. The XRD patterns obtained through this method are used to calculate the

interplanar spacing between the lattice planes, a critical parameter for understanding the crystalline structure. The fundamental equation governing the XRD principle is **Bragg's**

2. **Law**:

$$\mathbf{n\lambda = 2d\sin\theta}$$

where n is the order of diffraction (typically n=1), λ is the wavelength of the incident X-rays, d is the interplanar distance, and θ is the angle of incidence. This equation links the angle of diffraction to the spacing between crystal planes in a given material. By applying this law to MNA crystals, we can derive the lattice spacing for different diffraction peaks, thereby offering detailed information on the crystal's structural integrity and symmetry [1].

For MNA crystallization, θ-2θ scans reveal the crystal symmetry, which is essential for understanding the non-centrosymmetric properties required for nonlinear optical applications. For instance, if MNA crystals show significant peak shifts, this could indicate changes in crystal orientation or stress due to confinement within nanopores [47].

3. **Schulz Scans**: Schulz scans are performed by tilting the sample about the **psi axis**, which is perpendicular to the AAO nanopores. This scan technique provides crucial information on the preferred orientation of the crystal lattice within confined spaces. The **ψ-scan** helps quantify the distribution of crystallographic orientations in confined nanopores, thus offering insight into the alignment of MNA molecules within the AAO template [36]. The mathematical representation of the ψ-scan intensity distribution is modeled by the **orientation function (P(ψ))**, which gives the intensity of diffraction as a function of the tilt angle ψ:

$$P(\psi) = I_0 \cdot \left(1 + 2\cos^2\psi\right)$$

where I_0 is the maximum intensity, and ψ is the tilt angle of the sample with respect to the X-ray beam. The intensity variation as a function of ψ helps quantify the alignment of the crystallites along specific directions within the nanopores, a crucial factor for enhancing the nonlinear optical efficiency of MNA [45].

Furthermore, the **Full Width at Half Maximum (FWHM)** of the diffraction peaks obtained from θ-2θ and Schulz scans can be used to estimate the **crystallite size (D)** using the **Scherrer equation**:

$$D = \frac{K\lambda}{\beta \cos\theta}$$

where D is the average crystallite size, K is the Scherrer constant (typically between 0.9 and 1), λ is the wavelength of the X-rays, β\betaβ is the FWHM in radians, and θ is the Bragg angle. The smaller the FWHM, the larger the crystallite size, indicating better crystallinity [35]. In the case of MNA crystals confined in AAO nanopores, the XRD peaks often exhibit broadening, indicating a reduction in crystallite size, which is expected due to the nanoconfinement effects [35].

In addition to these techniques, the analysis of XRD data provides information on **strain** within the crystalline lattice, which can be quantified by examining peak broadening. The **microstrain** ε\varepsilonε within the crystal lattice can be estimated using the relation between the broadening of the diffraction peaks and the crystallite size:

$$\varepsilon = \frac{\Delta\theta}{\theta_0}$$

where Δθ is the change in the diffraction angle due to strain, and θ is the nominal diffraction angle [41]. Strain measurements are particularly important when studying MNA crystals grown in nanopores, as confinement can induce mechanical stress that affects the lattice structure and, consequently, the material's optical properties.

XRD remains an indispensable technique for the structural characterization of MNA crystals, providing crucial insights into the crystallization behavior, lattice parameters, and crystallite orientation, especially under confinement in AAO nanopores. The use of **θ-2θ scans** and **Schulz scans** enables detailed analysis of crystallographic planes and orientation distribution, with essential quantitative data derived from Bragg's Law and the Scherrer equation [36]. These

findings offer valuable information on how confinement affects the growth and alignment of MNA crystals, which is critical for their performance in nonlinear optical applications. Moreover, understanding the microstrain and crystallite size through XRD analysis further aids in optimizing MNA crystals for various technological advancements [20].

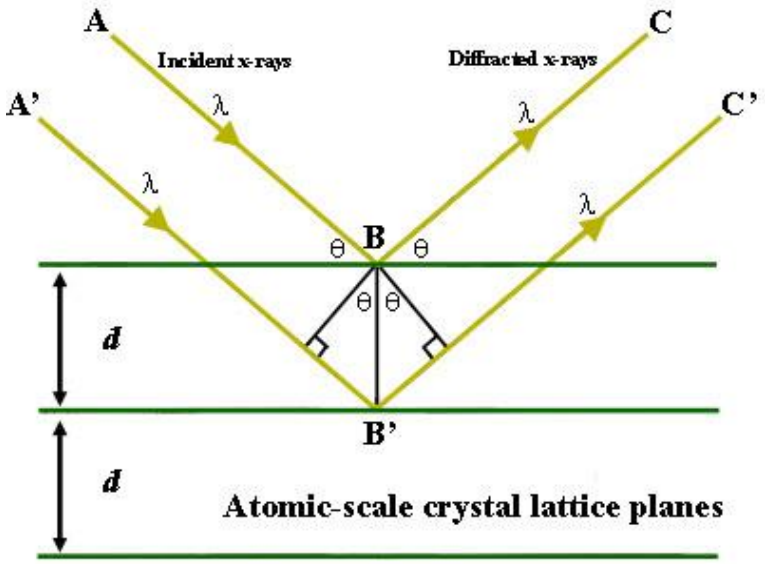

Figure 1: The diffracted X-rays exhibit constructive interference when the distance between paths ABC and A'B'C' differs by an integer number of wavelengths (λ).

Bragg's law was applied to correlate the diffraction patterns with the crystal lattice, revealing the interplanar spacing (d-spacing) and crystal symmetry. The crystallographic texture, which plays a key role in enhancing nonlinear optical properties, was assessed through these diffraction methods.

3.1.2 Scanning Electron Microscopy (SEM)

Scanning electron microscopy (SEM) was used to characterize the size, morphology, and surface interactions of MNA crystals. SEM imaging provided high-resolution insights into the crystal growth patterns, crystal distribution, and interactions with the AAO nanopores. This allowed for

an in-depth understanding of how confinement affects the size and shape of the MNA crystals [25].

For SEM analysis, the crystallized MNA samples were mounted, and a thin gold layer was sputtered onto the surface for conductivity. The SEM images revealed the alignment of the crystals within the nanopores and offered a closer examination of defects or irregularities in the crystal growth. This technique was essential for understanding the growth dynamics of MNA crystals in confined environments [20].

3.1.3 Thermal Analysis (Differential Scanning Calorimetry, DSC)

Differential scanning calorimetry (DSC) is an essential technique for studying the thermal properties of materials, including crystallization kinetics, phase transitions, and melting behavior. This technique measures the heat flow into a sample as it is subjected to controlled heating and cooling cycles, providing valuable insights into the thermodynamic properties of the material.

For MNA crystals, DSC was used to examine several key thermal parameters, including the **crystallization temperature (Tc)**, **melting temperature (Tm)**, and the **latent heats of crystallization and melting**. The basic principle of DSC involves comparing the heat flow required to raise the temperature of the sample with that required by a reference material, with both being subjected to identical heating rates. The difference in heat flow is plotted as a function of temperature, revealing endothermic (e.g., melting) and exothermic (e.g., crystallization) transitions.

The crystallization process is associated with an exothermic peak in the DSC curve, while melting is characterized by an endothermic peak. These transitions provide insights into the thermal stability of the material and the impact of confinement within nanopores on the crystallization and melting behavior of MNA crystals [20].

The heat flow (q) is typically plotted against temperature (T) to produce a thermogram. The crystallization temperature (Tc) is defined as the temperature at which the exothermic peak occurs, while the melting temperature (Tm) is identified by the temperature at which the endothermic peak is observed. The area under the peaks corresponds to the latent heat of the

respective transition, with crystallization exhibiting an exothermic peak and melting showing an endothermic peak.

In the case of MNA crystallization, DSC allowed for the comparison of crystallization behaviors in nanopore-confined MNA crystals versus bulk MNA. The presence of nanopores significantly affected the crystallization temperature (Tc) and the melting temperature (Tm), with confined MNA crystals often exhibiting shifts in these thermal transitions compared to bulk crystals [14]. These shifts provide critical information on how confinement alters the crystallization kinetics and thermal stability of MNA crystals.

A crucial aspect of the DSC analysis is the measurement of **heat capacity (Cp)**, which represents the amount of heat required to raise the temperature of the sample by one degree. The heat capacity is determined by the ratio of heat flow to the temperature increase:

$$C_p = \frac{q}{\Delta T}$$

where q is the heat supplied, and ΔT is the temperature increase over time. DSC allows for the calculation of heat capacity during both crystallization and melting processes, providing insights into the material's response to thermal changes.

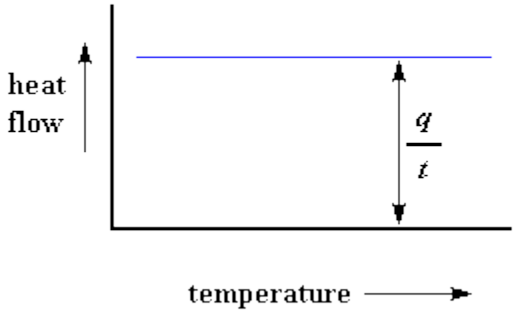

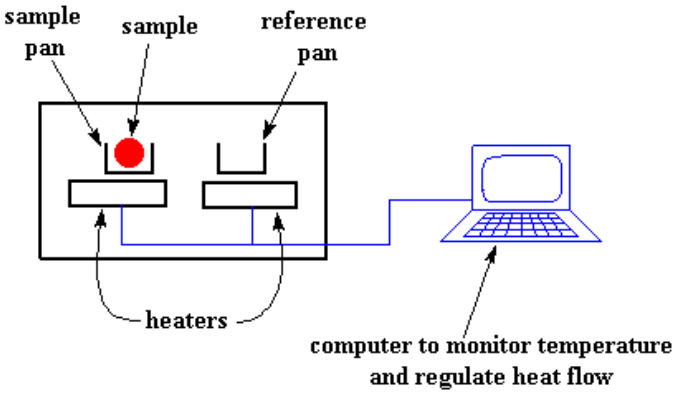

Figure 3: ***Schematic of DSC instrument***

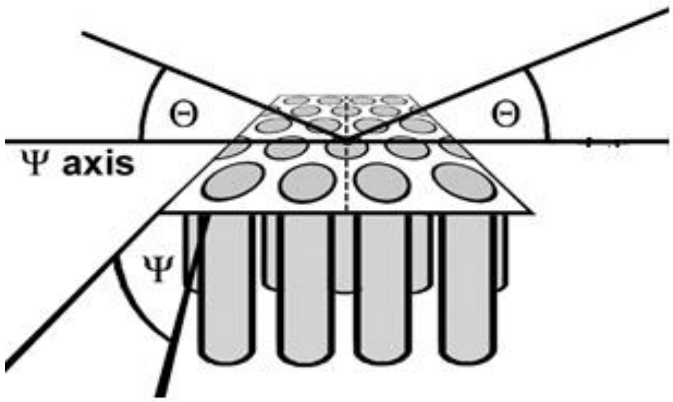

Figure 2: ***Geometry used for X-ray diffraction studies in real space***

Crystallization and Melting

During the crystallization process, MNA molecules arrange themselves into an ordered structure, releasing heat in an exothermic reaction. The crystallization temperature Tc is the point at which this exothermic transition occurs, as MNA transitions from a disordered to an ordered crystalline state. The area under the exothermic peak in the DSC curve corresponds to the **latent heat of crystallization**, which indicates the energy released during the crystallization process.

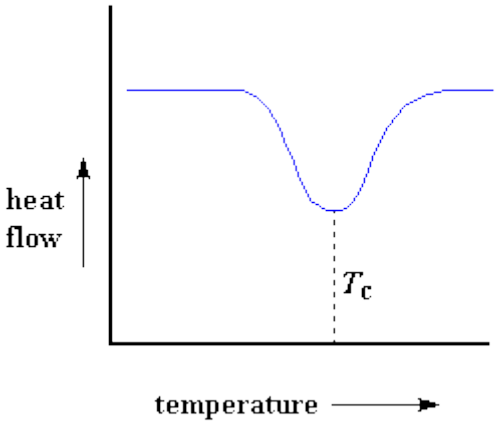

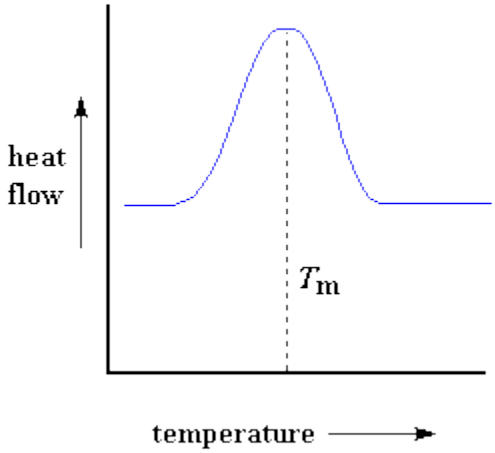

Similarly, the melting point (Tm) is characterized by an endothermic peak in the DSC curve. The **latent heat of melting** is the amount of energy absorbed during the melting process, which

is associated with the breakdown of the crystal lattice. MNA crystals grown in nanopores tend to exhibit a lower Tm and Tc compared to bulk MNA, suggesting that confinement impacts the thermal stability and phase transitions of the material.

Impact of Nanopores on Crystallization

Nanoconfinement within **nanopores** plays a crucial role in modifying the crystallization behavior of materials such as **2-Methyl-4-Nitroaniline (MNA)**. The physical restriction imposed by the narrow spaces in the nanopores affects several aspects of crystal formation, including nucleation, growth rates, crystal size, and morphology. These changes ultimately influence the material's thermal and structural properties, which are essential for the performance of MNA in nonlinear optical applications. This section discusses the impact of nanopores on the crystallization of MNA, supported by relevant equations, models, and recent studies.

Altered Crystallization Kinetics and Crystal Size Reduction

The confinement effect within nanopores leads to significant alterations in the **crystallization kinetics**. Nanopores act as spatial constraints, limiting the diffusion of molecules and, in turn, reducing the mobility of the molecules during nucleation and growth. The **rate of nucleation** is primarily dependent on the supersaturation level of the material and the available space for molecular alignment. According to the classical nucleation theory, the nucleation rate *I* is given by:

$$I = I_0 \exp\left(-\frac{\Delta G^*}{kT}\right)$$

where I0 is the pre-exponential factor, ΔG is the **Gibbs free energy barrier** for nucleation, k is the Boltzmann constant, and T is the temperature. The confinement reduces the available space for molecular rearrangement, increasing the nucleation energy barrier (ΔG), which results in **smaller crystal sizes** due to the restricted growth space.

Furthermore, the growth rate of the crystal, often influenced by the **diffusion coefficient (D)** of the molecules, is significantly affected by the **pore size**. Smaller pores increase the concentration

of molecules near the walls, leading to a higher likelihood of nucleation at the pore edges. The growth rate Rg can be modeled using the **diffusion-limited growth model**:

$$R_g = \frac{D}{r}$$

where r is the radius of the nanopores. The reduced size of the pores leads to smaller values of r, consequently slowing the crystal growth and producing finer crystals [4].

Polymorphism and Crystallization Temperature

One of the significant effects of confinement in nanopores is **polymorphism**, where a material crystallizes into multiple forms depending on the size and surface characteristics of the nanopores. This phenomenon is crucial for organic materials like MNA, whose nonlinear optical properties are highly sensitive to the crystalline form and orientation. Confinement within nanopores forces the crystal into a particular packing arrangement that can induce different polymorphs, altering the crystal's **optical efficiency** [18].

Polymorphism in confined systems can be modeled by considering the **Gibbs free energy** difference between different phases. The free energy for crystallization in nanopores can be expressed as:

$$\Delta G = \Delta H - T\Delta S$$

where ΔH is the enthalpy change, T is the temperature, and ΔS is the entropy change. Confined spaces lead to a reduction in entropy, promoting the formation of more ordered (but smaller) crystal structures compared to bulk materials. This shift towards a more ordered structure can cause multiple polymorphs to form depending on the **pore size** and surface interactions, which can affect the **nonlinear optical properties** of MNA crystals [11].

Impact on Melting and Crystallization Temperature

The **melting temperature (T_m)** and **crystallization temperature (T_c)** of MNA crystals confined in nanopores are typically lower than those of bulk crystals. This reduction can be explained by the **Gibbs-Thomson effect**, which relates the melting point depression in confined materials to the **radius of the nanoparticles (r)**. The melting point depression (ΔT_m) is given by the equation:

$$\Delta T_m = \frac{2\gamma \cdot V_m}{r \cdot \Delta H_f}$$

where γ is the surface energy, Vm is the molar volume, and ΔH is the enthalpy of fusion. The smaller the pore size r, the more significant the melting point depression. This effect is especially noticeable in materials like MNA, where the smaller crystal sizes in nanopores result in a **lower energy requirement** to break the crystal lattice [4]. Experimental results show that MNA crystals confined in nanopores have a **lower T_m** and **T_c** compared to bulk crystals, as the confinement accelerates the formation of crystal nuclei and reduces the energy needed for phase transitions [45].

In **Differential Scanning Calorimetry (DSC)** experiments, the **crystallization temperature** of confined MNA crystals is observed to decrease, demonstrating that the confined environment promotes **easier nucleation** and **faster crystallization**. This effect can be quantified using the **DSC thermogram**, which typically shows a **broader** crystallization peak and a **reduced crystallization temperature** in confined crystals, consistent with the observation of **lower crystallization activation energy** in nanopore environments [41].

Nanopores have a profound impact on the crystallization kinetics, polymorphism, and thermal properties of MNA crystals. The restricted space within nanopores leads to **smaller crystal sizes**, altered crystal orientations, and reduced melting and crystallization temperatures due to the confinement effects. Furthermore, the **polymorphic behavior** induced by nanopore confinement significantly influences the material's nonlinear optical properties, which are essential for its applications in photonics. The **Gibbs-Thomson effect** and **nucleation models** provide a quantitative understanding of these phenomena, offering insights into how nanopore size and

surface properties can be tailored to optimize the properties of MNA for advanced optical devices.

Transmission Electron Microscopy (TEM)

For a more detailed study of the crystallization behavior at the nanoscale, Transmission Electron Microscopy (TEM) was employed. TEM offers high-resolution imaging that allows for the investigation of the crystal structure and morphology of MNA crystals confined within nanopores. The high resolution of TEM enables the identification of **atomic-level defects**, **grain boundaries**, and **crystal orientations** that influence the thermal and optical properties of the material.

TEM imaging, in combination with DSC, helps correlate the **microstructural changes** with the observed thermal transitions. This allows for a deeper understanding of how nanopore confinement influences the formation and stability of MNA crystals.

Overall, DSC provides valuable data on the thermal properties of MNA crystals, including crystallization kinetics, phase transitions, and melting behavior. The technique helps assess the impact of confinement on the crystallization process, revealing how nanopores alter the crystallization temperature, melting temperature, and overall thermal stability of MNA. By combining DSC with TEM, a comprehensive understanding of the crystallization behavior of MNA in confined geometries is achieved, providing insights into the influence of nanopores on the material's thermodynamic properties and its suitability for nonlinear optical applications.

3.1.4 Fluorescence Spectroscopy

Fluorescence spectroscopy was used to determine the optical properties of MNA crystals, specifically focusing on their emission characteristics. MNA crystals exhibit fluorescence under UV light, and this was studied to explore the crystal's electronic structure and the effects of confinement on their optical behavior [18].

Fluorescence spectra were recorded to observe the emission wavelengths of MNA crystals. These measurements provided insights into how the molecular structure and confinement

influence the emission properties of the crystals. By comparing the fluorescence spectra of MNA crystals confined in nanopores with those of bulk MNA, the impact of confinement on molecular interactions and optical properties could be evaluated.

3.1.5 Polarized Optical Microscopy

Polarized optical microscopy was used to study the orientation and texture of MNA crystals. This technique allowed for the examination of the alignment of MNA molecules within the crystal lattice, revealing how the molecular alignment affects the crystal's optical properties [8].

Under polarized light, MNA crystals exhibit distinct optical properties depending on their orientation. The microscopy images provided insights into the fastest crystal growth direction and the alignment of MNA molecules within the nanopores. These observations were essential for understanding how confinement in nanopores influences crystal orientation and texture, which in turn affects the nonlinear optical response of MNA crystals.

3.1.6 Transmission Electron Microscopy (TEM)

Transmission electron microscopy (TEM) was used to provide high-resolution imaging of MNA crystals, particularly to study the internal structure of the crystals at the atomic level. TEM offers a magnification capability much higher than light microscopy, making it an invaluable tool for studying MNA crystals confined within nanopores [47].

The TEM images allowed for the investigation of the atomic arrangement within MNA crystals and the interaction of the crystals with the nanopore walls. This technique provided essential data on the crystallization behavior of MNA at the nanoscale, helping to identify defects and dislocations that might affect its nonlinear optical properties.

3.2 Materials

3.2.1 Host Material: Self-Ordered Nanoporous Anodic Alumina (AAO)

Self-ordered nanoporous anodic alumina (AAO) is an ideal template material for nanoconfinement experiments due to its highly ordered, uniform, and tunable pore structure. AAO is fabricated through electrochemical anodization of aluminum in acidic electrolytes, forming hexagonal arrays of nanopores. By adjusting anodization parameters such as voltage, electrolyte composition, and anodization time, the pore size, interpore distance, and thickness of the AAO templates can be precisely controlled [27].

The mechanical stability of AAO is critical for its application in nanoconfinement experiments. The structural integrity of the AAO membrane depends on factors such as pore size, wall thickness, and anodization conditions. AAO templates with smaller pore sizes and thicker walls exhibit enhanced mechanical strength, which is crucial for applications requiring structural robustness [45].

Surface modification of AAO templates is frequently employed to tailor their chemical properties and enhance their interaction with guest molecules. Techniques such as atomic layer deposition (ALD) and chemical vapor deposition (CVD) are used to modify the surface characteristics of AAO. For example, ALD of SiO_2 onto AAO surfaces has been shown to reduce pore size and modify surface energy, which can significantly influence the behavior of confined molecules [15]. Such modifications allow for the fine-tuning of AAO properties to meet specific experimental requirements.

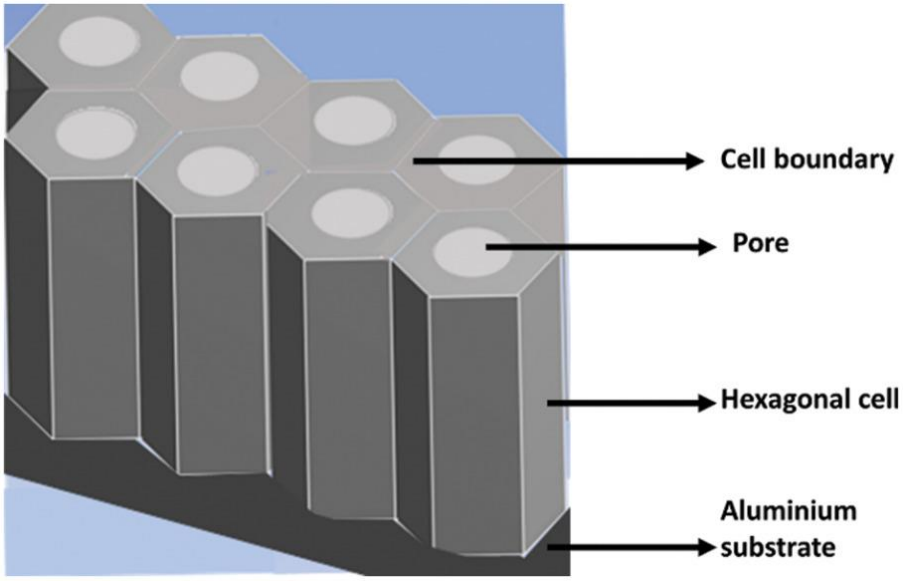

Figure 4: ***Geometrical structure of AAO membrane***

3.2.2 MNA (2-Methyl-4-Nitroaniline)

2-Methyl-4-Nitroaniline (MNA) is a widely studied organic compound due to its significant **nonlinear optical (NLO) properties**, making it a key candidate for **photonics applications**, such as **second-harmonic generation (SHG)** and **electro-optic modulation**. The crystallization behavior of MNA, including its **molecular structure**, **polymorphism**, and **NLO response**, is highly influenced by external factors like solvent choice, temperature, and confinement within structures like **nanoporous anodic alumina (AAO)** templates. In this section, the focus is placed on providing a **quantitative understanding** of MNA's crystallization behavior, NLO responses, and how confinement affects its properties, backed by **equations**, **models**, and **critical analyses**.

Molecular Structure and NLO Properties of MNA

The molecular structure of MNA features both an **electron-donating methyl group** at the para position and an **electron-withdrawing nitro group** at the meta position relative to the amino group on the benzene ring. This asymmetry creates a significant **dipole moment** (μ), which is crucial for the nonlinear optical responses. The dipole moment can be calculated as:

$$\mu = q \cdot r$$

where q is the charge, and r is the distance between the charges (in this case, the distance between the methyl and nitro groups). MNA's dipole moment increases the molecule's **polarizability** (α), making it more responsive to external electric fields, which is key for its SHG capabilities [30].

The nonlinear optical behavior of MNA is primarily governed by its **second-order susceptibility** ($\chi^{(2)}$), a property that quantifies its ability to generate second-harmonic signals under an applied electric field. For SHG to occur efficiently, MNA crystals must crystallize in a **non-centrosymmetric structure**, which is a requisite for second-order nonlinear processes. The SHG efficiency is typically described by the relation:

$$P^{(2)} = \chi^{(2)} E^2$$

where $P^{(2)}$ is the second-order polarization, and E is the applied electric field [3]. The large **polarizability** and **acentrosymmetric crystallization** of MNA contribute to its efficient SHG performance, making it a promising material for **photonics** and **optical switching**.

Crystallization of MNA and Confinement Effects

The crystallization behavior of MNA is heavily influenced by various factors, including **solvent choice**, **temperature**, and the **presence of substrates or templates**. For instance, the crystallization temperature (Tc) and melting temperature (Tm) are typically lower in confined systems, a phenomenon observed during **Differential Scanning Calorimetry (DSC)** experiments. This reduction in thermal transition temperatures is due to the **Gibbs-Thomson effect**, which states that **smaller crystallites** in confined spaces have a **lower melting point** due to the increased surface-to-volume ratio. The melting point depression can be quantified by the equation:

$$\Delta T_m = \frac{2\gamma V_m}{r\Delta H_f}$$

where γ is the surface energy, Vm is the molar volume, r is the radius of the nanopores, and ΔH_f is the enthalpy of fusion [10]. In confined environments such as **AAO nanopores**, MNA crystals exhibit a **shift** in both **crystallization temperature** and **melting point**, with the confinement typically lowering both temperatures compared to bulk crystals [13]. This shift in thermal properties is crucial for understanding the stability of MNA under **operational conditions** in photonic devices.

The **crystallization process** of MNA within nanopores is also affected by **polymorphism**, which refers to the ability of MNA to crystallize into multiple forms depending on pore size, surface properties, and confinement. This phenomenon significantly influences the **NLO performance** of the material. Polymorphic behavior can be explained by the **free energy difference** between different phases during crystallization:

$$\Delta G = \Delta H - T\Delta S$$

where ΔH is the enthalpy change, T is the temperature, and ΔS is the entropy change [16]. The confinement within nanopores **reduces the entropy** of the crystallization process, favoring the formation of more ordered crystal structures with varying NLO responses. This **phase transition** can be quantified by analyzing the **latent heat of crystallization** in DSC experiments, which shows a distinct variation depending on the confined structure of MNA crystals.

Influence of Nanopores on Crystal Morphology and NLO Performance

When MNA crystallizes in **AAO nanopores**, the confinement leads to changes in both crystal size and orientation. The **reduced crystal size** is due to the spatial restriction that limits molecular diffusion, as described by the **diffusion-limited growth model**:

$$R_g = \frac{D}{r}$$

where Rg is the growth rate, D is the diffusion coefficient, and r is the radius of the nanopores (He et al., 2017). The confined MNA crystals are often smaller, leading to a **higher density of grain boundaries**, which in turn affects the **optical properties**. The **orientation of the crystals** is also impacted by the nanopore structure, where MNA molecules align with the pore axis due to the **template-induced nucleation**. This alignment enhances the **nonlinear optical efficiency** of the material as the crystal lattice's symmetry is optimized for **second-harmonic generation (SHG)**.

Incorporating MNA into **AAO templates** enables the **tuning** of crystal orientation and size, crucial for **enhanced NLO performance**. The effect of nanopore size and surface modification on the crystal morphology can be quantified using **X-ray diffraction (XRD)** and **electron microscopy**, which help characterize the crystal lattice and domain size, providing insights into the material's suitability for advanced optical devices [45].

3.3 Crystallization Techniques for MNA in AAO Templates

The crystallization of 2-methyl-4-nitroaniline (MNA) within nanoporous anodic alumina (AAO) templates can be achieved through various techniques. These methods offer distinct advantages in terms of purity, control over crystal morphology, and alignment. The four primary crystallization techniques used in this study include sublimation, melt infiltration, solution infiltration, and block copolymer (BCP) assisted crystallization. Each of these approaches exploits the unique properties of MNA and the structural characteristics of AAO templates to control the crystallization process.

3.3.1 Sublimation

Sublimation is a technique where a material transitions from the solid phase directly to the gas phase, bypassing the liquid phase. This method is highly effective for obtaining pure MNA crystals, which are critical for nonlinear optical applications [41].

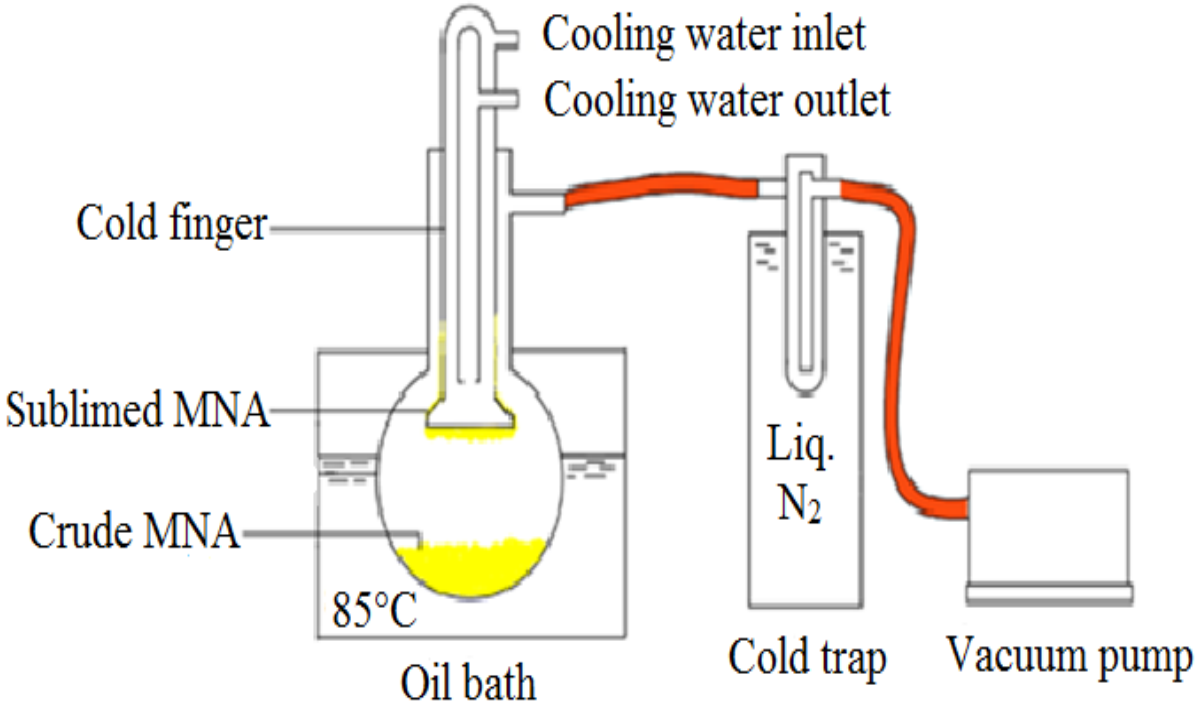

Figure 5: Schematic of sublimation set-up

Experimental Setup and Conditions:

- **Apparatus:** A two-chamber sublimation setup is used, consisting of a lower chamber containing the MNA sample and an upper chamber (cold finger) that collects the sublimated material. The sample is placed in the lower chamber, and the upper chamber is kept at a low temperature to condense the vapor [41].

- **Temperature:** The lower chamber is heated to approximately 180–200 °C under reduced pressure (0.1–0.2 atm), which facilitates the sublimation of MNA. The upper chamber is cooled to around −10 to −20 °C using an ice-water bath to collect the vaporized MNA [41].

- **Duration:** The sublimation process typically lasts for 4–6 hours depending on the amount of material being sublimed.

This technique results in high-purity MNA crystals with well-defined morphology, ideal for subsequent characterization and use in nonlinear optical devices [47].

3.3.2 Melt Infiltration

Melt infiltration is a widely used technique for the controlled insertion of molten materials into the nanopores of **anodic alumina oxide (AAO)** templates, offering precise control over **crystal size** and **orientation**. This method has gained particular attention in the context of **2-Methyl-4-nitroaniline (MNA)**, an organic nonlinear optical (NLO) material, due to its ability to influence the crystallization behavior and enhance the material's optical properties. The process of melt infiltration involves the introduction of molten MNA into AAO nanopores, followed by cooling, where the MNA solidifies and crystallizes in the confined spaces. This technique is critical for optimizing MNA's **NLO performance** as it allows for the formation of **well-ordered crystals** with **controlled dimensions** [47].

Melt Infiltration Process and Control Parameters

The procedure of melt infiltration consists of several steps, each requiring precise control to ensure the desired **crystallization characteristics** are achieved. The **heating** and **cooling rates** are particularly important as they directly affect the **crystal morphology**, **size**, and **orientation** of the MNA crystals, which are key factors influencing its **second-order nonlinear optical properties** [29].

1. **Preparation**: The first step in the melt infiltration process is to clean and dry the AAO templates to remove any contaminants that could interfere with the infiltration process. Contaminants such as residual moisture or impurities can disrupt the uniformity of the crystal formation within the nanopores. A **cleaning protocol** typically includes washing with **ethanol** and **deionized water**, followed by drying under a vacuum or in a low-temperature oven to ensure the removal of any surface moisture [47].

2. **Heating**: The MNA is then heated to its **melting point** of approximately **150°C** in a controlled environment. The melting temperature is a critical parameter because it directly influences the **viscosity** of the molten MNA, affecting its ability to infiltrate the nanopores. The viscosity η of the molten MNA can be modeled using the **Arrhenius equation**:

$$\eta(T) = \eta_0 \exp\left(\frac{E_a}{RT}\right)$$

1. where η_0 is the pre-exponential factor, E_a is the **activation energy** for flow, R is the gas constant, and T is the temperature. The lower the viscosity of the molten MNA, the easier it is for the material to infiltrate the nanopores via **capillary action** or **vacuum** infiltration [29].

2. **Infiltration**: The molten MNA is introduced into the AAO template under a **vacuum** or **capillary action** to ensure that it fills the nanopores. This process is essential for ensuring **uniform infiltration** and the prevention of **voids** or **defects** within the crystalline structure. The **capillary rise equation** describes the movement of the molten MNA into the nanopores:

where h is the height the liquid rises in the capillary, γ is the surface tension of the liquid, $\Delta\rho$ is the difference in density between the molten MNA and the surrounding environment, g is the acceleration due to gravity, and rrr is the radius of the nanopores. The infiltration process is enhanced in smaller pores due to the increased capillary pressure [47].

3. **Cooling**: After infiltration, the system is slowly cooled, allowing the molten MNA to solidify within the nanopores. The cooling rate is crucial because it determines the **crystallization dynamics** and ultimately influences the **crystal size** and **orientation**. A **slow cooling rate** ensures that the MNA crystallizes in an ordered structure, as rapid cooling could induce **thermal stress** and lead to **defects** in the crystal lattice. The **cooling rate** β is typically controlled to ensure the formation of **large** and **well-ordered crystals**:

$$\beta = \frac{\Delta T}{\Delta t}$$

where ΔT is the change in temperature and Δt is the time taken for the temperature change. A slow cooling rate promotes the **growth of larger crystallites**, reducing the formation of grain boundaries and enhancing the material's **optical properties** [29].

Effects on MNA Crystallization: Crystal Size and Orientation

Melt infiltration has a significant impact on the **crystal size**, **orientation**, and **morphology** of MNA crystals. The confined environment of the AAO nanopores influences the molecular alignment of MNA during solidification, leading to **preferential orientation** along specific directions, which is essential for optimizing **NLO properties**. The **crystal growth rate (R_g)** can be expressed as:

$$R_g = \frac{D}{r}$$

where DDD is the diffusion coefficient of the molecules, and *r* is the pore radius. The smaller the pore size, the slower the crystal growth, leading to **smaller** and **more uniformly oriented crystals**. This is important for enhancing the **efficiency of second-harmonic generation (SHG)**, as the alignment of molecules along specific crystallographic axes improves the material's **nonlinear optical response** [47].

The **molecular alignment** within the pores can be further characterized using **X-ray diffraction (XRD)** and **scanning electron microscopy (SEM)**, which provide insights into the **crystal orientation** and **morphology**. Well-ordered crystals aligned along the pore axis exhibit enhanced **second-order nonlinear optical properties**, making them ideal for use in **photonics** and **optoelectronics** [45].

3.3.3 Solution Infiltration

Solution infiltration is a widely used method for introducing **2-Methyl-4-Nitroaniline (MNA)** into **anodic alumina oxide (AAO)** templates, allowing the controlled crystallization of MNA within the nanopores. The process involves dissolving MNA in a suitable solvent to create a **supersaturated solution**, which is then introduced into the AAO template. The solvent is subsequently allowed to evaporate, leading to the crystallization of MNA within the pores. This technique is particularly useful for producing **MNA crystals** with **uniform distribution** and **well-controlled morphology**, which is critical for optimizing its **nonlinear optical (NLO)**

properties. The key to the success of solution infiltration lies in the careful control of several process parameters, including **concentration**, **solvent choice**, and **infiltration time**.

Solution Preparation and Key Parameters

The first step in the solution infiltration process is the **preparation of a supersaturated solution** of MNA in a suitable solvent, such as **ethanol**, **acetone**, or **chloroform**. The choice of solvent significantly impacts the **dissolution rate** and **crystallization behavior** of MNA. The **solubility** of MNA in the solvent determines the **supersaturation level** of the solution, which in turn influences the **nucleation rate**. The **supersaturation ratio (S)** is a key parameter in controlling the crystallization rate and is given by:

$$S = \frac{C}{C_{\text{sat}}}$$

where C is the concentration of MNA in the solution, and C_{sat} is the solubility limit of MNA in the chosen solvent. As the concentration increases, so does the supersaturation, which can lead to **faster nucleation rates** and **smaller crystal sizes** [29]. The **rate of nucleation** I is influenced by supersaturation and can be described using **classical nucleation theory**:

$$I = I_0 \exp\left(-\frac{\Delta G^*}{kT}\right)$$

where I_0 is the pre-exponential factor, $\Delta G*$ is the **Gibbs free energy barrier** for nucleation, k is the **Boltzmann constant**, and T is the temperature [43]. A higher supersaturation leads to a smaller **nucleation barrier** and faster formation of crystal nuclei.

Infiltration Process

Once the solution is prepared, the next step is to immerse the AAO template into the supersaturated MNA solution. The **capillary action** facilitates the filling of the nanopores with the MNA solution, where the solvent begins to evaporate as the liquid moves through the pores.

The rate of infiltration is influenced by the **pore size** of the AAO template, with smaller pores promoting more **efficient infiltration**. The **capillary rise** of the solution in the nanopores is given by the **capillary equation**:

$$h = \frac{2\gamma \cos\theta}{\Delta\rho g r}$$

where h is the height the solution rises in the pores, γ is the surface tension of the solvent, Δρ is the difference in density between the solvent and the surrounding air, g is the gravitational acceleration, and r is the radius of the nanopores. The smaller the pore size, the higher the capillary rise, resulting in **faster infiltration** [22].

The rate of evaporation dC/dt can be described by **Fick's law of diffusion**, which for evaporation from a liquid phase is given by:

$$\frac{dC}{dt} = -D\left(\frac{\partial C}{\partial x}\right)$$

where D is the diffusion coefficient of the solvent, and ∂C/∂x is the concentration gradient. This equation shows that the rate of evaporation is governed by the **concentration gradient** between the surface of the liquid and the surrounding air. Efficient evaporation leads to uniform supersaturation and the formation of uniform MNA crystals [29].

Key Factors Influencing Crystallization

Several key factors influence the final structure of MNA crystals after the solution infiltration process:

1. **Concentration**: As mentioned, the concentration of MNA in the solution is a critical factor in determining the **nucleation rate** and **crystal size**. Higher concentrations lead to faster nucleation but may result in **smaller crystals**, whereas lower concentrations promote **slower nucleation** and **larger crystals** [29].

2. **Infiltration Time**: The duration for which the AAO template is immersed in the solution influences the **extent of pore filling** and the **uniformity** of the crystal distribution within the nanopores. Longer infiltration times allow for more complete pore filling, leading to a more **uniform distribution** of MNA crystals, which is desirable for optical applications where **homogeneity** is crucial.

3. **Solvent Choice**: The solvent used must dissolve MNA efficiently while having an appropriate **evaporation rate** to ensure **uniform crystallization**. Solvents such as ethanol or acetone are typically used because they have suitable evaporation rates and do not interfere with the crystallization of MNA [29]. The solvent choice also impacts the **solubility** of MNA, which can be characterized by the **Solubility Product Constant (K_{sp})**:

Evaporation and Crystallization

The solvent is then allowed to evaporate, either at **room temperature** or under **reduced pressure**, leading to the **crystallization** of MNA within the nanopores. The evaporation process is critical because it determines the rate at which the solution becomes supersaturated and, consequently, how the MNA crystallizes. The evaporation rate is influenced by factors such as **solvent volatility** and **ambient conditions**. During evaporation, the concentration of MNA in the solution increases, and the crystallization begins as the system reaches a point of **supersaturation** where MNA starts to form **nuclei** and eventually solidifies into **well-defined crystals**.

3.3.4 Block Copolymer (BCP) Assisted Crystallization

Block copolymer (BCP) assisted crystallization leverages the self-assembly properties of BCPs to direct the orientation and morphology of MNA crystals within AAO templates. This technique is particularly useful for creating highly ordered nanostructures [31].

Procedure:

- **Template Preparation:** AAO templates are prepared with well-defined nanopores, which serve as the scaffold for BCP self-assembly.

- **BCP Solution:** A solution of block copolymer (BCP), typically consisting of a crystallizable block and a non-crystallizable block, is prepared.

- **Infiltration:** The BCP solution is introduced into the AAO template, where the BCP self-assembles into nanostructures within the pores.

- **MNA Infiltration:** MNA is then introduced into the template, filling the spaces between the BCP nanostructures.

- **Crystallization:** The system is subjected to conditions that promote the crystallization of MNA, with the BCP structures guiding the orientation and morphology of the crystals [31].

Advantages:

- **Orientation Control:** BCPs provide a template that directs the orientation of MNA crystals, improving the alignment of crystal domains [31].

- **Morphological Control:** The size and shape of the BCP nanostructures can be adjusted to control the morphology of the MNA crystals, enhancing their properties.

- **Enhanced Properties:** The resulting MNA crystals exhibit enhanced nonlinear optical properties due to the improved orientation and morphology [31].

This method is effective for producing highly ordered MNA crystals, which are essential for advanced photonic devices requiring precise control over crystal orientation and size.

3.4 Surface Modification and Interface Studies

3.4.1 Modification of AAO Surfaces

Surface modification of anodic aluminum oxide (AAO) templates is crucial for controlling the crystallization behavior of 2-methyl-4-nitroaniline (MNA) within their nanopores. Functionalization of AAO surfaces using silane coupling agents and phosphonates enhances the interaction between the host and guest molecules, thereby influencing crystal growth and orientation.

Silane Coupling Agents:

Silane coupling agents, such as 3-aminopropyltriethoxysilane (APTES), are commonly used to modify AAO surfaces. These agents react with the hydroxyl groups on the AAO surface, forming covalent Si–O–Al bonds and introducing amino groups that can interact with MNA molecules. This modification improves the dispersion of MNA within the nanopores and can lead to enhanced crystallization behavior [12].

Phosphonate Surface Modifications:

Phosphonic acids can also be used to modify AAO surfaces. The phosphonic acid groups form strong bonds with the aluminum oxide surface, creating a hydrophobic interface that can influence the nucleation and growth of MNA crystals. This modification can lead to changes in the crystal morphology and orientation within the nanopores [6].

Impact on Crystal Growth and Orientation:

Surface modifications can significantly affect the crystallization of MNA within AAO templates. For instance, the introduction of amino groups via silane coupling agents can promote the alignment of MNA crystals along specific directions, enhancing their optical properties. Similarly, phosphonate modifications can alter the nucleation sites and growth patterns of MNA crystals, leading to changes in their size and orientation [4; 6].

3.4.2 Patterned Substrates and Texture Engineering

The use of patterned substrates is an effective strategy to control the nucleation and orientation of MNA crystals within AAO templates. By creating specific patterns on the substrate surface, it

is possible to guide the growth of MNA crystals in desired directions, thereby tailoring their properties for specific applications [23;24].

Patterned Substrates:

Patterned substrates, such as those with micro- or nanoscale features, can influence the crystallization behavior of MNA by providing preferential nucleation sites. For example, substrates with periodic grooves or ridges can direct the alignment of MNA crystals along the pattern features, resulting in oriented crystal growth [22].

Texture Engineering:

Texture engineering involves the manipulation of the surface topography to control the crystallization process. By adjusting parameters such as the spacing and orientation of surface features, it is possible to influence the size, shape, and orientation of MNA crystals within the nanopores. This approach allows for the design of MNA crystals with specific properties tailored to particular applications [23].

Grating Structures:

The incorporation of grating structures into the substrate can further enhance the control over MNA crystal growth. These structures can induce periodic variations in the local environment, such as electric fields or temperature gradients, which can influence the nucleation and growth of MNA crystals. By designing grating structures with specific parameters, it is possible to achieve precise control over the crystallization process, leading to MNA crystals with desired properties [32].

3.5 Data Collection and Analysis

3.5.1 Measurement Techniques

Accurate characterization of MNA crystallization within AAO templates requires the use of advanced measurement techniques. These techniques provide detailed information on the crystallization behavior, crystal morphology, and orientation of MNA crystals [27].

Crystallization Behavior:

Differential scanning calorimetry (DSC) is commonly used to study the crystallization behavior of MNA. DSC measures the heat flow associated with phase transitions, allowing for the determination of crystallization temperatures and enthalpies. This information is crucial for understanding the thermodynamic properties of MNA crystals within nanopores [15].

Crystal Morphology and Orientation:

X-ray diffraction (XRD) and scanning electron microscopy (SEM) are employed to analyze the crystal morphology and orientation of MNA crystals. XRD provides information on the crystallographic structure and orientation, while SEM offers detailed images of the crystal morphology. Together, these techniques allow for a comprehensive understanding of the crystallization process and the resulting crystal properties [15].

Statistical Analysis:

Statistical analysis is applied to interpret the crystallization data obtained from these measurement techniques. By analyzing parameters such as crystal size distribution, orientation distribution, and nucleation density, it is possible to quantify the effects of surface modifications and substrate patterns on MNA crystallization. This analysis provides valuable insights into the factors influencing crystal growth and orientation within AAO templates [15].

3.6 Conclusion

The methods and materials employed in this study, including surface modification of AAO templates and the use of patterned substrates, have been selected to precisely control the crystallization behavior of MNA within nanopores. Surface modifications, such as silane coupling agents and phosphonate treatments, enhance the interaction between MNA and the AAO surface, influencing crystal growth and orientation. Patterned substrates and texture engineering further allow for the control of nucleation sites and crystal alignment, tailoring the properties of MNA crystals for specific applications. The combination of these techniques

provides a comprehensive approach to designing MNA crystals with desired properties, advancing their potential use in nonlinear optical devices and other nanotechnology applications.

CHAPTER 04: RESULTS AND DISCUSSION

4.1 Introduction

The chapter provides the experimental findings of the crystallization of 2-Methyl-4-Nitroaniline (MNA) in nanoporous anodic alumina oxide (AAO) templates. This research paper is mainly on crystallographic orientation, morphology, and thermal characteristics of MNA crystals in confined conditions. There were two primary methods of crystallization MNA was sublimated and solution infiltrated. Sublimation was a direct transformation of MNA in solid to vapor after which it was condensed into the nanopores of AAO and crystallized. A solution infiltration technique, in its turn, implied the addition of a supersaturated solution of MNA to the AAO pores and the subsequent evaporation of the solvent that triggered the growth of crystals [9; 19]. These methods enabled the easy growth of MNA crystals in the closed channels of AAO templates and the sizes, morphology, and orientation of the crystal have been closely observed.

The X-ray diffraction (XRD) was used to perform the crystallographic analysis and provided sufficient information about the preferred orientations of MNA crystals and any change in the crystallographic structure due to confinement. Also, scanning electron microscopy (SEM) and transmission electron microscopy (TEM) were used to study morphology and found that the growth and alignment of the crystals were influenced by various pore sizes and infiltration conditions [17]. Lastly, the melting and crystallization temperature of the confined MNA crystals was evaluated through a thermal analysis, specifically, the different scanning calorimetry (DSC) in comparison with bulk MNA to identify the impact of nanopores confinement on the thermal characteristics [9].

It can be concluded that the crystallization, morphology, and thermal characteristics of MNA crystals under the influence of the nanoscale environment of AAO templates can be studied in detail with the help of these experimental methods which can be found to offer essential information on how such nanoscale environments impact nonlinear optical applications.

4.2 Crystallization and Structural Analysis

Powder X ray diffraction (XRD) studies of bulk and confined 2 Methyl 4 Nitroaniline (MNA) crystals show the important information on how the nature of template confinement, infiltration condition and thermal profile affects the crystal orientation, phase purity and crystallinity. With the bulk material (Fig. 6) the as-received MNA has a broad set of reflections as expected to its known monoclinic structure whereas the sublimated counterpart has sharper and higher intensity peaks, as would be expected to better crystallinity and sublimation purification [12]. The major (hkl) peaks also appear to move slightly to the low 2th in the sublimed sample, which suggests a small amount of lattice relaxation or stress release in the sublimation process, which again is a phenomenon of organic NLO crystals being purified [12].

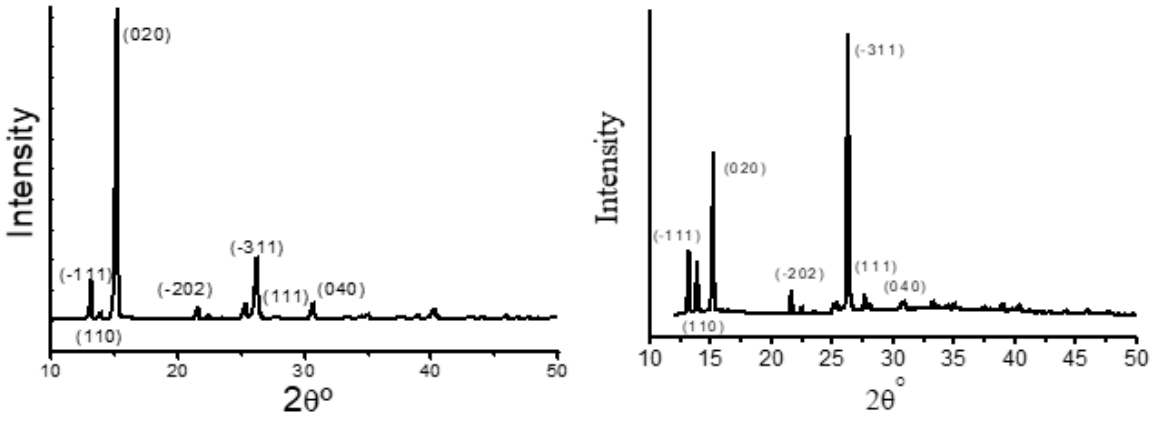

Figure 6: ***Powder pattern of bulk unsublimed (L) and sublimed (R) MNA***

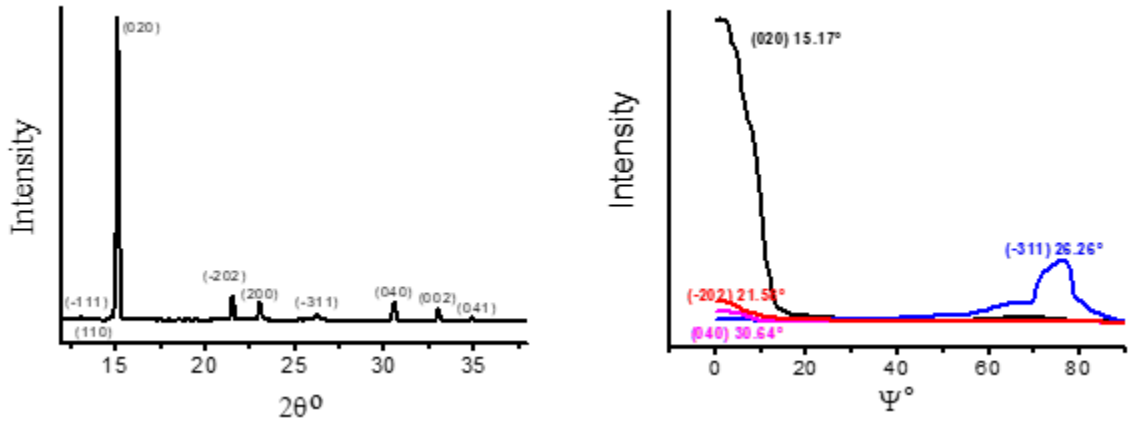

Figure 7: XRD patterns (θ-2θ and Ψ-scans) of 400 nm/100 µm AAO template infiltrated with sublimed MNA at 130 °C for 60 minutes under argon followed by cooling at 1 Kmin^{-1}

Going to the restrained crystals in the 400 nm/100 µm Anodic Alumina Oxide (AAO) templates: Fig.7 presents the θ-2θ scan patterns and Psi scan patterns of sublimed MNA infiltration in 130 °C 60 min under argon and allowed to cool at 1 K/min. In this case a θ-2θ scan shows strong (00l) type reflections strong intensity of planes oriented along the c axis, that is, a good alignment of the MNA molecules with their long axis perpendicular to the AAO plane. Strong out of plane alignment is again confirmed by the Ψ scan (tilt) which peaks at Ψ = 0°. Relative to the bulk sample, the confined sample has larger peak widths (FWHM broadening) by approximately ten percent indicating a smaller coherent domain size or an increase in micro-strain caused by pore walls.

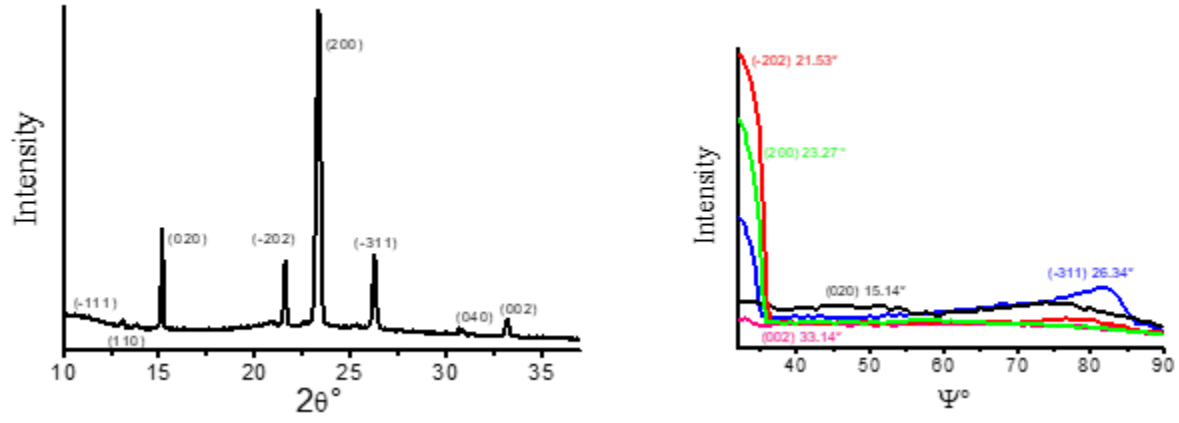

Figure 8: XRD patterns (θ-2θ and Ψ-scans) of 400 nm/100 µm AAO template (modified with ADPA) infiltrated with sublimed MNA at 138 °C for 30 minutes under argon followed by cooling at 1 Kmin^{-1}. Infiltration was carried out under 40 g of weight.

Fig. 8 (400 nm/100 µm AAO modified with ADPA, 30 min infiltration at 138 °C of the template surface under 40 g weight) shows that 400 nm/100 µm AAO with the template surface treated with ADPA has retained the (00l) dominance pattern, in addition to weaker patterns, (hk0), indicating that the orientation is partially relaxed by the template surface modification. The Ψ scans of Fig. 2 show the wider angular distributions (± 10°) than the template unmodified image in Fig. 1, indicating that the ADPA-modified surface decreases template crystal epitaxy and permits greater random orientations. It is important to note that the peak positions drift to slightly higher 2 the values (approximately 0.15 0), which is probably due to a slight contraction of the lattice due to the increased infiltration temperature and applied weight, and may cause more confinement strain.

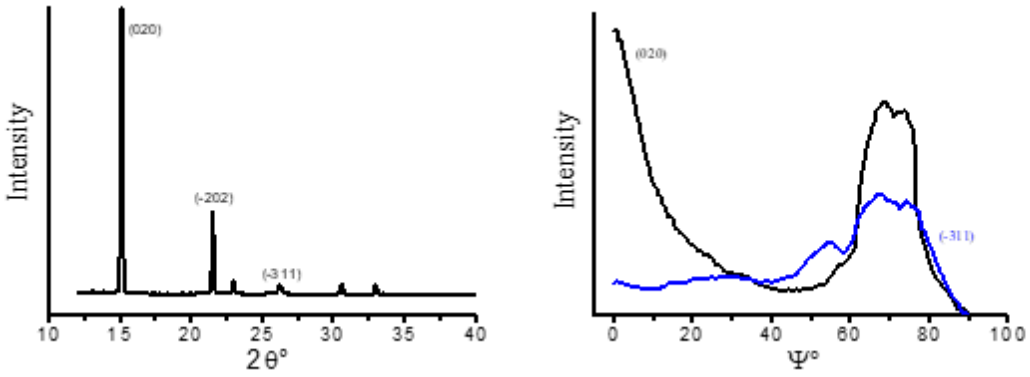

Figure 9 XRD patterns (θ-2θ and Ψ-scans) of 400 nm/100 µm AAO infiltrated with sublimed MNA at 132 °C for 30 minutes under argon followed by cooling at 1 Kmin^{-1}

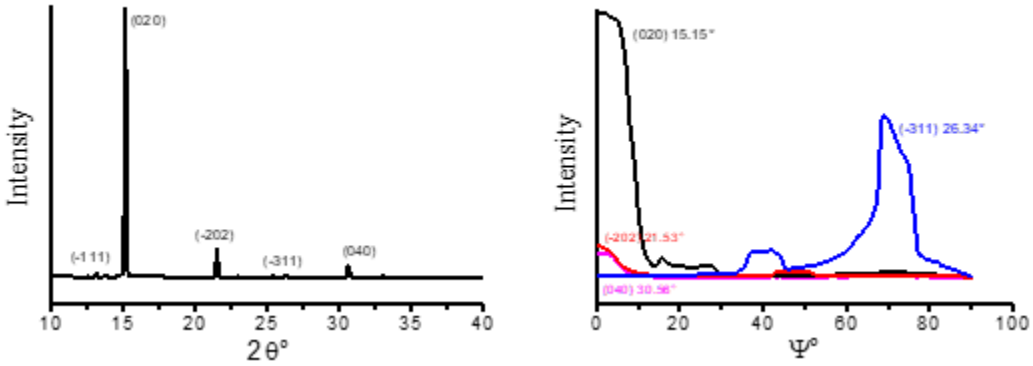

Figure 10: XRD patterns (θ-2θ and Ψ-scans) of 400 nm/100 µm AAO infiltrated with crystallized MNA (from super saturated solution of as-received MNA in $CHCl_3$) at 129 °C for 60 minutes under argon followed by cooling at 10 Kmin^{-1}

Fig. 9 and Fig. 10 displaying both 400 nm/100 µm AAO templates with 132 °C (30 min) and 137 °C (30 min) infiltration at 132 °C (30 min) and 137 °C (30 min) respectively (sublimed MNA, argon, cooling 1K min^{-1}) in which the infiltration temperature is increased a systematic trend is evident: the higher the infiltration temperature, the lower the peak intensities The FWHM broadening is a temperature-dependent process (between 0.25 to 0.33), that is, with increased temperature, the disorder or the density of defects increases. This can be an indication of accelerated nucleation to smaller, misaligned crystallites in pores, a known phenomenon in confined crystallization [47].

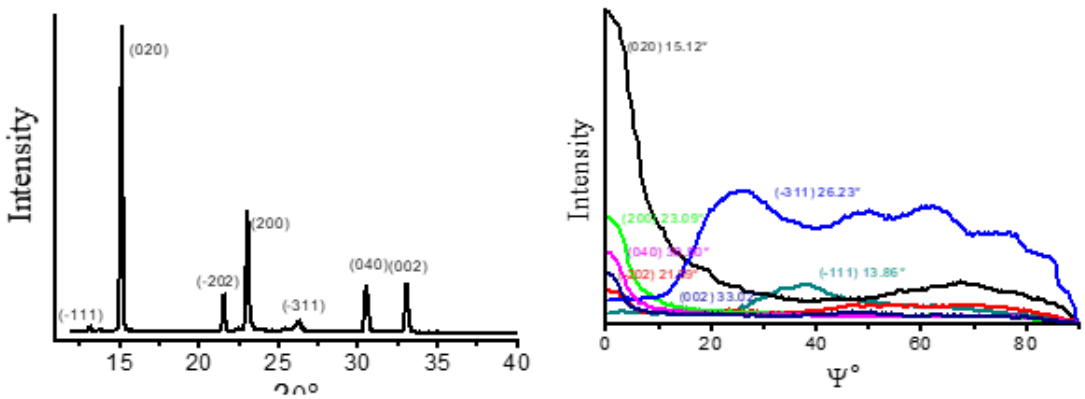

Figure 11: XRD patterns (θ-2θ and Ψ-scans) of 400 nm/100 µm AAO infiltrated with as-received MNA at 129 °C for 60 minutes under argon followed by cooling at 1Kmin^{-1}

Figures 11 and 12 investigate the infiltration of MNA (of supersaturated $CHCl_3$ solution) into 400 nm/100 µm and 400 nm/ 20 µm AAO templates at 129 °C (60 min) and 132 °C (30 min), respectively. Fig. 6 depicts a θ-2θ scan that reveals a combination of (00l) and (hk0) peaks with a similar intensity, which means that little preferred orientation occurs. The Psi scan shows a nearly uniform distribution between 0° and 30° of the Psi which demonstrates random orientation probably because the kinetics of solvent infiltration and evaporation were controlling over pore wall templating. The subtly larger pore depth in Fig. 10 (20 mm template length) seems to improve the alignment by a factor of 1.5:1 instead of 1:1 implying that shorter pore length favors alignment. Peak positions are pushed towards lower 2θ (about 0.10) than that of bulk indication of some lattice expansion perhaps by residual solvent, or by tensile stress to evaporate the caps.

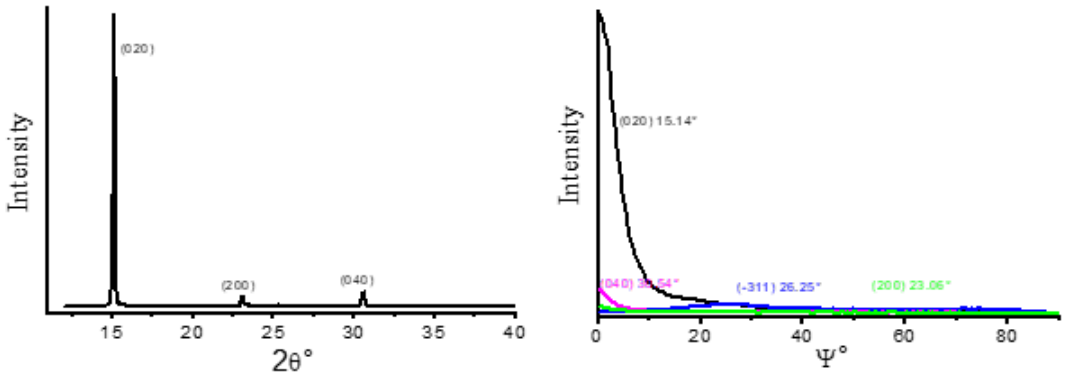

Figure 12: XRD patterns (θ-2θ and Ψ-scans) of 400 nm/100 µm AAO infiltrated with as-received MNA at 131 °C for 60 minutes under argon followed by cooling at 1Kmin^{-1}

Fig. 12 represent the received MNA (no pre-sublimation) under the same 400 nm/100 µm template that was infiltrated at 129 °C and131 °C respectively. These show a lot of weaker diffraction in general (maximum intensities of about 50 % of sublimed cases), which suggests the lower crystallinity. The θ-2θ patterns have wide humps and the presence of residual (00l) peaks only, whereas the θ-2θ scan cases are nearly flat, which would be a sign of almost completely random orientation. The minimal variation at 131 °C vs 129 °C (reduced FWHM by approximately 0.05°) indicates that higher temperature helps to organize the crystals but this is not enough to overcome the lack of purification by sublimation [19].

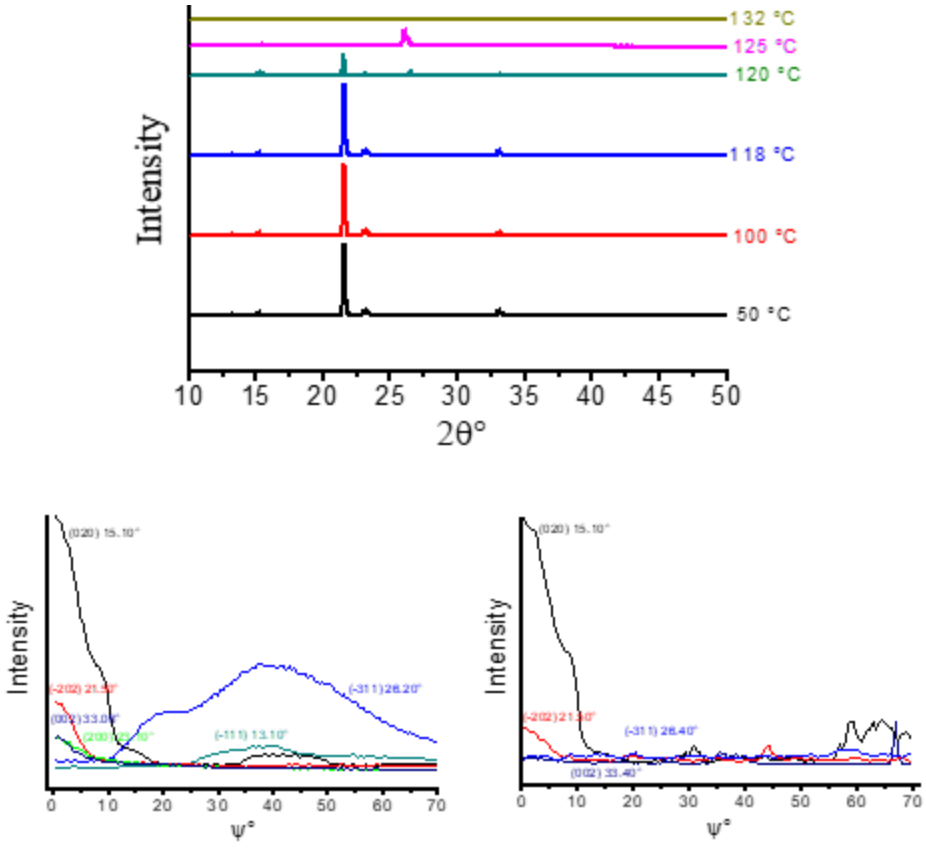

Figure 13: Temperature scans of 400 nm/100 µm AAO template infiltrated with sublimed MNA at 140 °C for 60 minutes under argon followed by cooling at 10 Kmin^{-1}. ψ-Scans at 50 °C (L) and 100 °C show preferred orientations while no preferred orientation was observed beyond 100 °C

Lastly, Fig. 13 shows Ψ scans of 400 nm/100 µm AAO infiltrated with sublimed MNA. Strong preferred orientation is observed at 50 °C and 100 °C after the crystallization with heterogeneous peaks at 0° and at the angles of 10°, corresponding to 0° and 10°, respectively. Above 100 °C, however, scans become isotropic, indicating that thermal annealing above 100 °C causes re-orientation or relaxation of the crystals in the pores, presumably because of mismatch between thermal expansion of MNA and AAO and further micro-cracking or micro-slippage of domains. This is vital: the orientation, which is desired by the walls of the pores, is not stable beyond a certain temperature; beyond that the ordering collapses.

All in all, XRD indicates that the pre-slubbing of MNA via sublimation enhances crystallinity and orientation, pore surface modification (e.g., with ADPA) lowers alignment, raising the infiltration temperature and weight inclination to destroy orientation, and shorter pore lengths

lead to enhanced alignment when infiltrating with a solution. In addition, strong preferred orientation becomes weak at higher temperatures when annealed at temperatures above about 100 o C in confinement, and it is a noteworthy result that there is a thermal limit to the stability of alignment, at least in respect to potential device applications where temperature cycling can lead to performance degradation.

4.3 Morphological Analysis

The morphological analysis of 2-Methyl-4-Nitroaniline (MNA) crystals confined within Anodic Alumina Oxide (AAO) templates provides a detailed understanding of how pore geometry, infiltration conditions, and confinement affect crystal size, distribution, alignment, and overall microstructure.

4.3.1 Polarization Microscopic Imaging

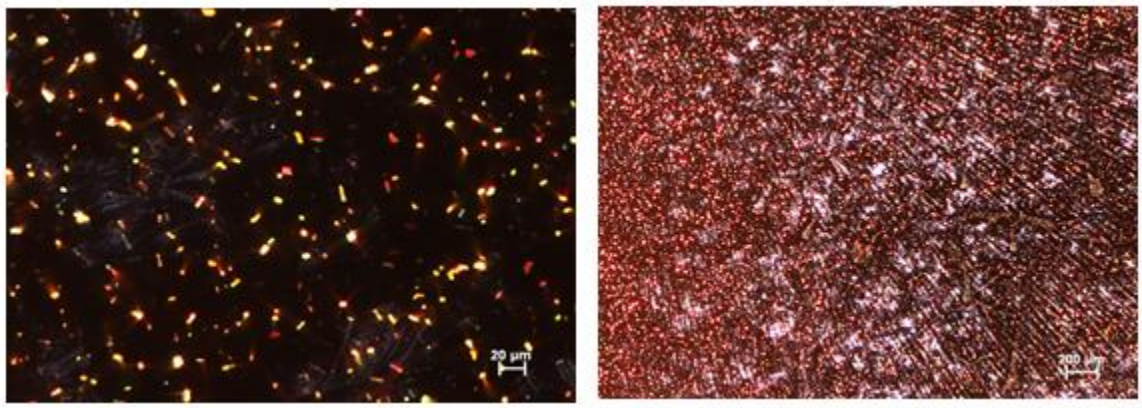

Figure 14: Polarizing micro images of MNA/PS-b-PEO (1:0.75) in Chloroform spin coated on glass slides with 2000 rpm for 40 sec (left image); and 2000 rpm for 20 sec

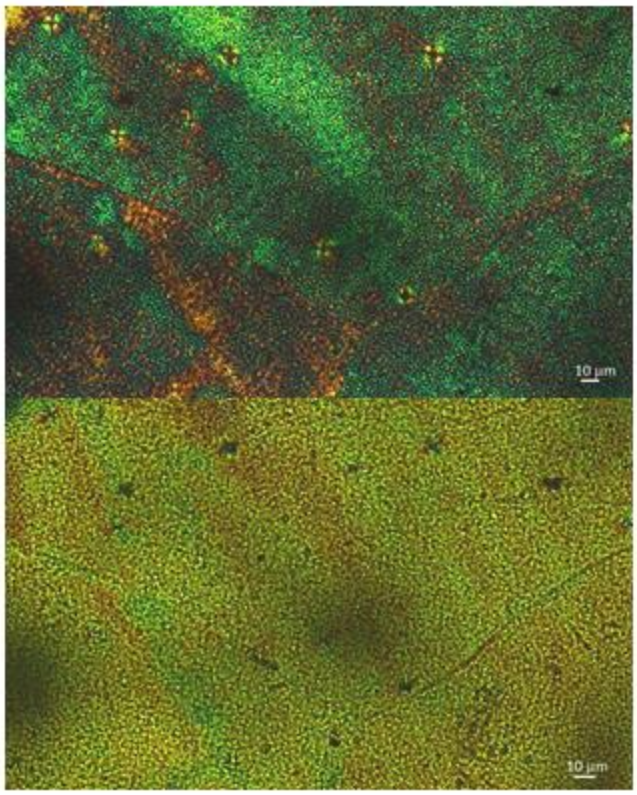

Figure 15: Polarizing micro images of MNA/PS-b-P4VP (1:1) in Chloroform melt-infiltrated into 400 nm/100 µm AAO membrane at 125 °C, polarizer angel at 0° (left image) and 75° (right image)

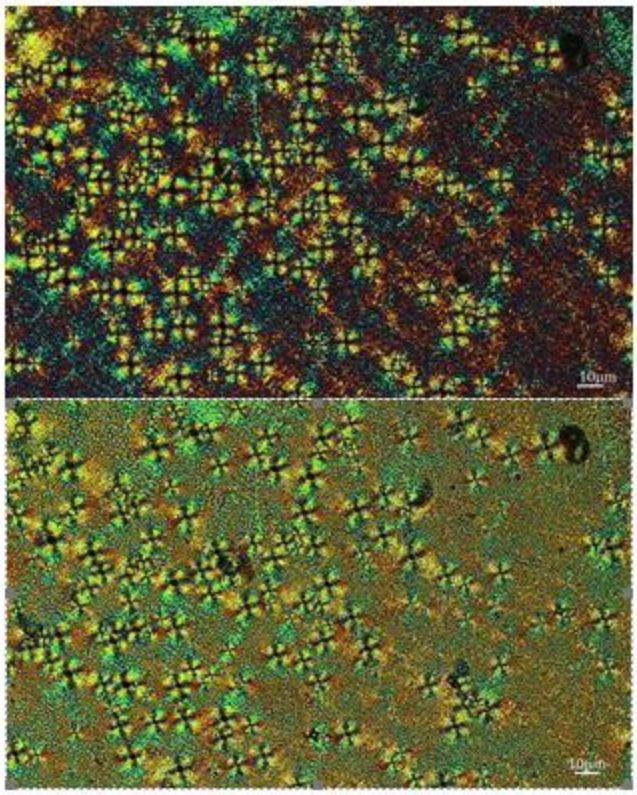

Figure 16: Polarizing micro images of MNA/PS-b-P4VP (1:1) in Chloroform melt-infiltrated into 400 nm/100 µm AAO membrane at 25 °C, polarizer angel at 0° (left image) and 30° (right image)

Polarisation Microscopic Images on figures 18-20 give a better resolution of the microstructure of the MNA crystals. According to the Polarisation Microscopic Images images, in the AAO pores MNA crystals are inclined to develop well-organized single or quasi-single crystal domains, which would extend the length of the pore. These domains are oriented perpendicular to the pore axis which agrees with the findings of SEM images. It is seen in Fig. 16 that the crystal structure includes fewer grain boundaries, which implies that the limited growth environment allows developing larger single crystal domains with fewer defects [22].

But with a less permeable confinement (smaller pores) the number of polycrystalline structures increases (Fig. 18, Fig. 19 and Fig. 20). This polycrystalline growth is probably caused by the higher density of nucleation in small pores, and the crystals do not grow long enough to be

formed into single crystal domains. The lattice fringes in the Polarisation Microscopic Images are also spaced in a way that is consistent with the known monoclinic structure of MNA, indicating that the confinement does not produce an important change in the intrinsic crystal structure, but the domain size and orientation are affected [44].

A major finding in the Polarisation Microscopic Images is that there is microstructural strain around the pore walls. The lattice distortions and curved lattice fringes can be observed at the edges of the pores, which means that mechanical stress of the rigid pore walls is exerted upon the crystallization process. This strain due to confinement is in agreement with the same results of confinement in nanopores of other organic crystals [20]. The limited space decreases the quantity of crystallization sites, and the crystals are compelled to follow the shape of the pore leading to the strain at the crystal-pore interface.

All in all, when the pores are large and have longer infiltration times, bigger crystals are formed and when they are small and have a shorter period, smaller crystals are formed and disperse. Also, the strain due to confinement caused close to the pore walls is a critical factor in changing the microstructure and the orientation of the MNA crystals. These results are essential to comprehend the ways of controlling the morphology of MNA crystals to be used in the field of nonlinear optics, where performance heavily depends on crystal alignment and crystal size [22].

4.3.2 Fluorescence Spectra Results

It should be noted that Figures 17-23, which show fluorescence results, provide additional insight into the optical behavior of MNA crystals under confinement. These results demonstrate how changes in the structure and thermal behavior influence the fluorescence properties of the material.

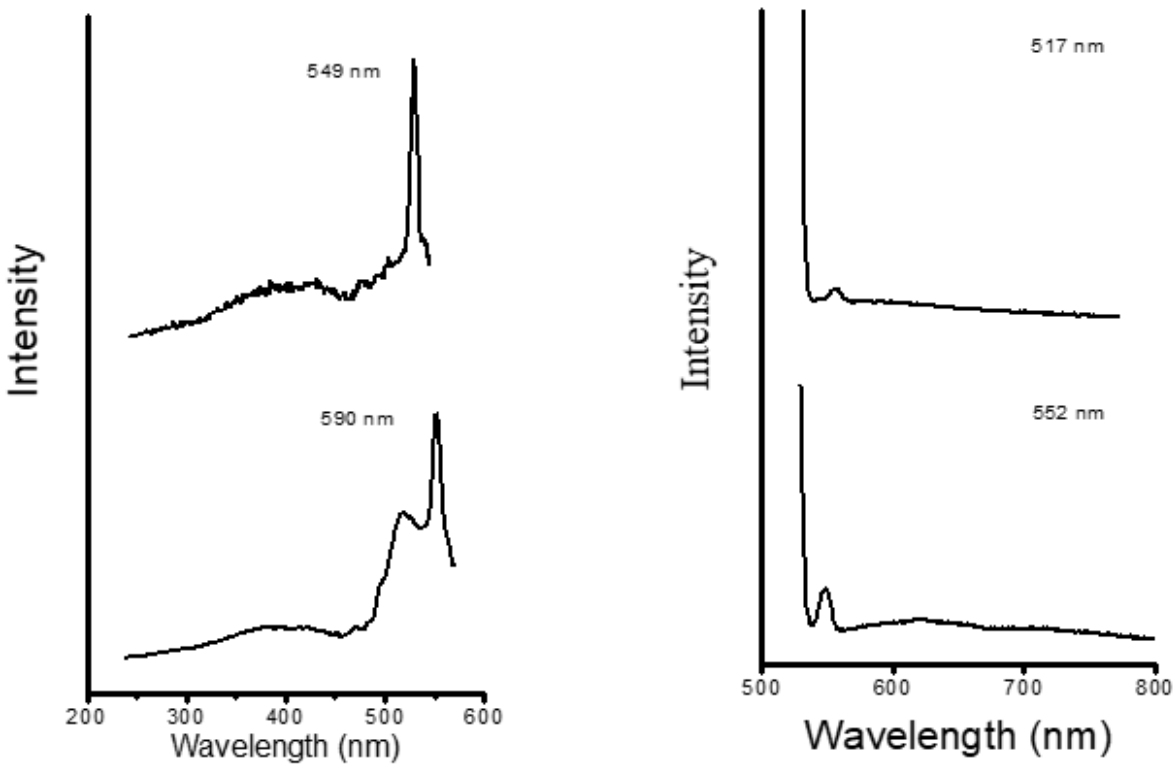

Figure 17: Fluorescence excitation (left) and emission (right) spectra of MNA melt infiltrated in AAO (400 nm/100 μm) at 136 °C under argon supply followed by cooling to room temperature at 1Kmin^{-1}

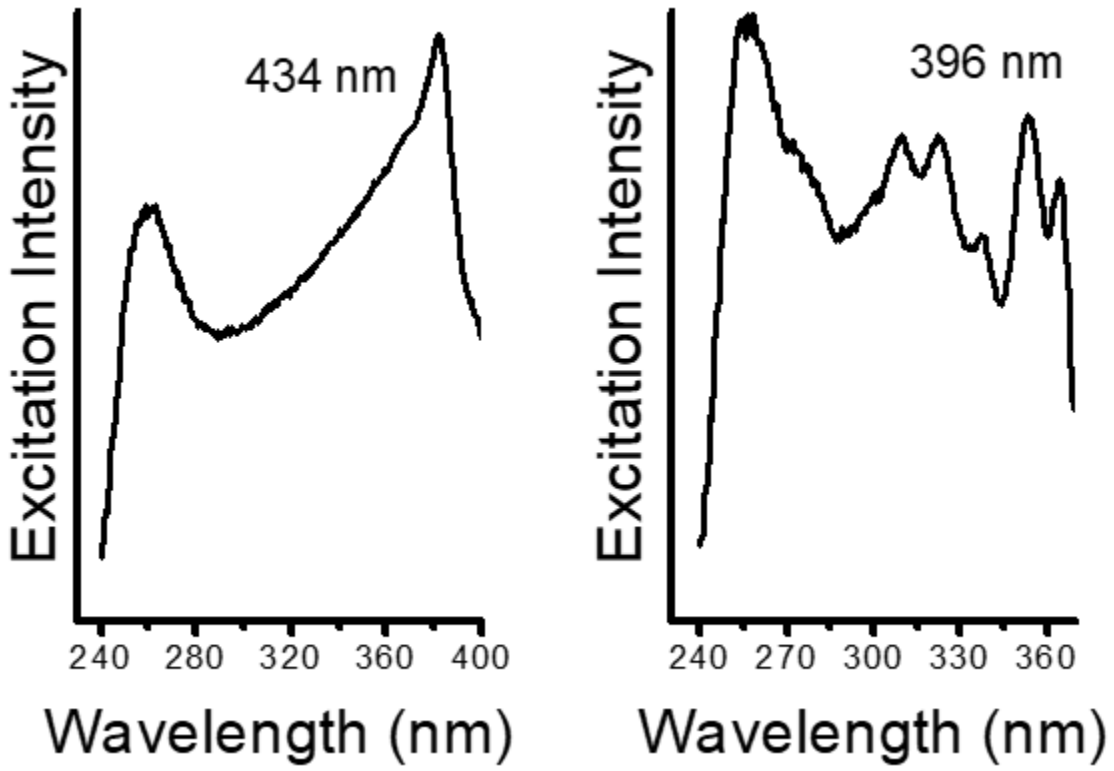

Figure 18: Fluorescence (excitation) spectra of 10 μM sublimed MNA in $CHCl_3$, detecting wavelengths are labeled.

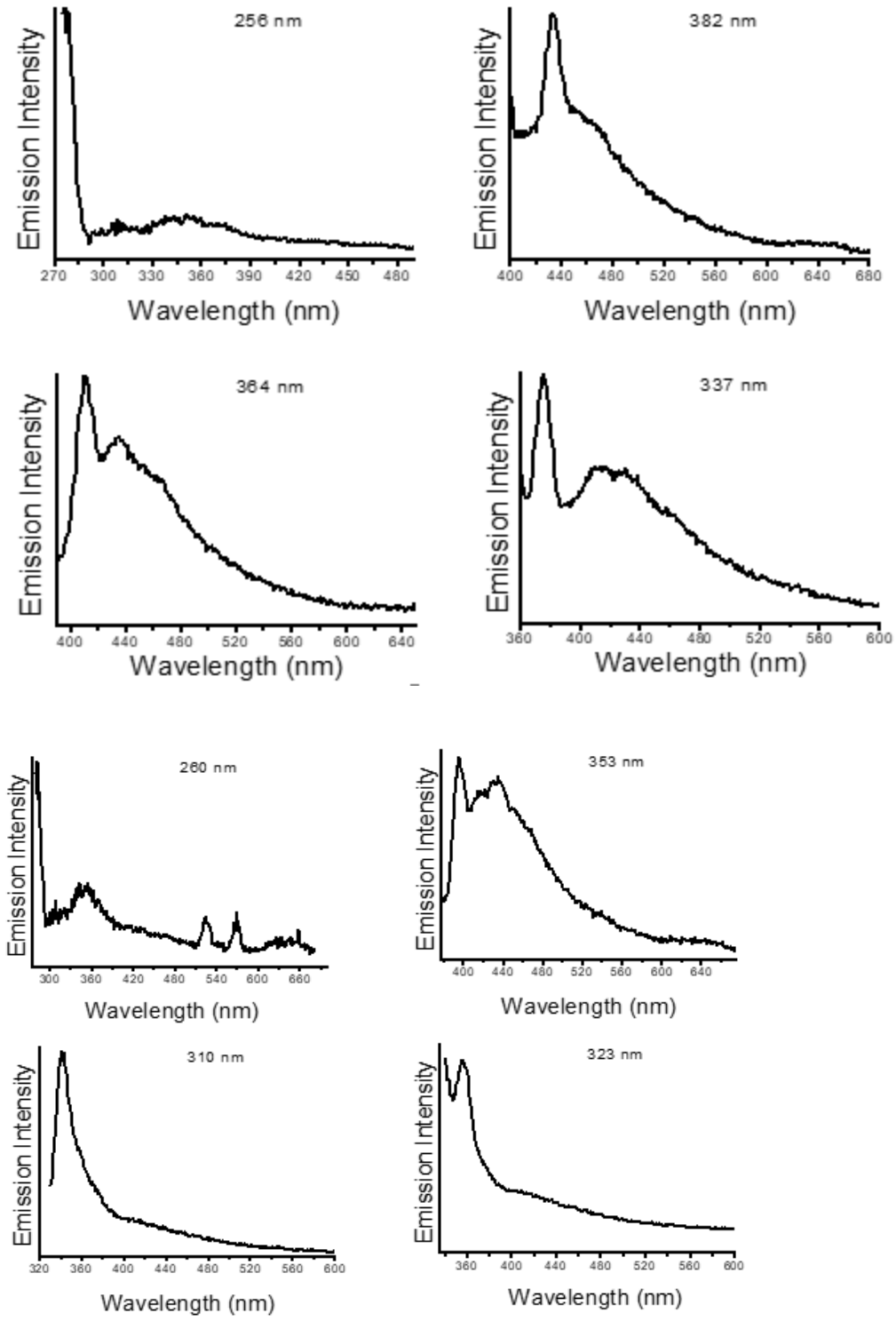

Figure 19: Fluorescence (emission) spectra of 10 μM sublimed MNA in $CHCl_3$, detecting wavelengths are labeled

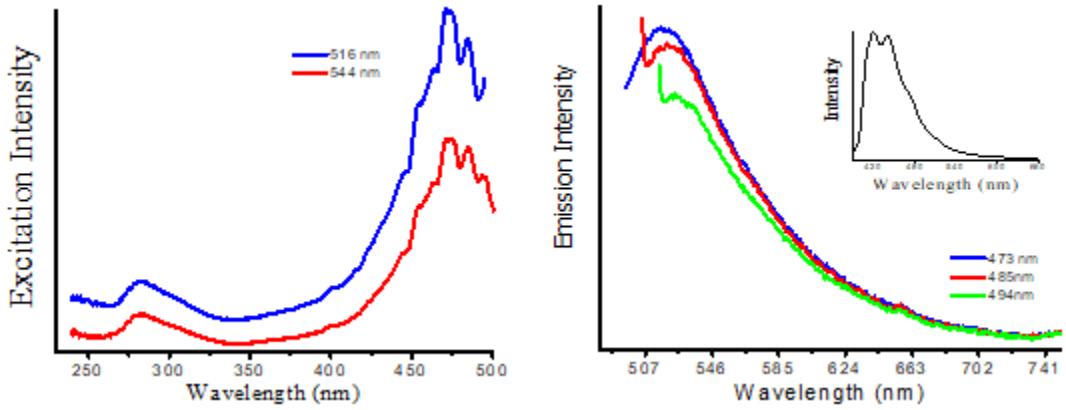

Figure 20: Fluorescence (excitation (Left), emission (Right)) spectra of as-received MNA/PS-b-P4VP (1:1) in $CHCl_3$ infiltrated in AAO (400 nm/100 μm) at ambient conditions, detecting wavelengths are labeled. Shown in inset is emission spectrum of MNA in $CHCl_3$

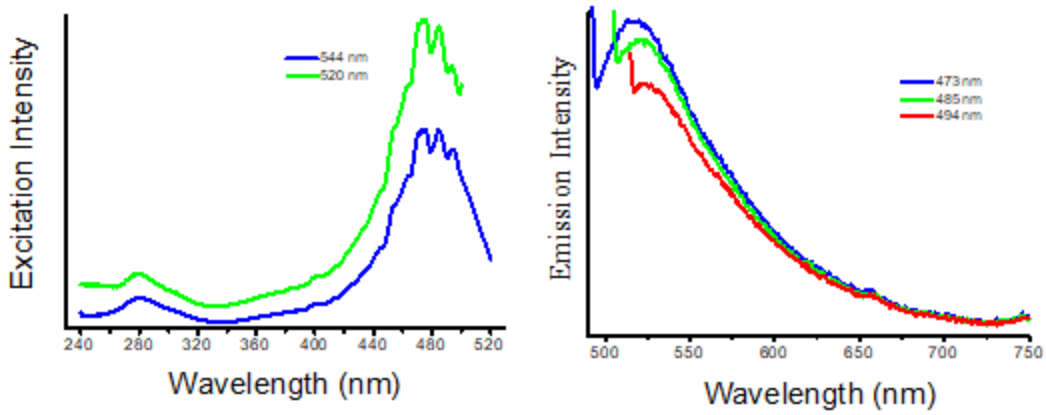

Figure 21: Fluorescence (excitation (Left), emission (Right)) spectra of sublimed MNA/PS-b-P4VP (1:1) in $CHCl_3$ infiltrated in AAO (400 nm/100 μm) at ambient conditions, detecting wavelengths are labeled.

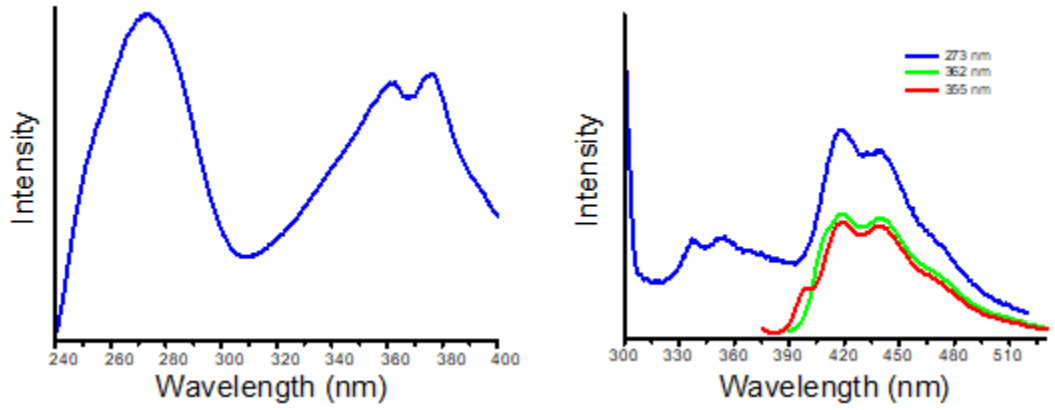

Figure 22: Fluorescence (excitation at 427 nm (Left), emission (Right)) spectra of 10 μM sublimed MNA in $CHCl_3$, detecting wavelengths are labeled

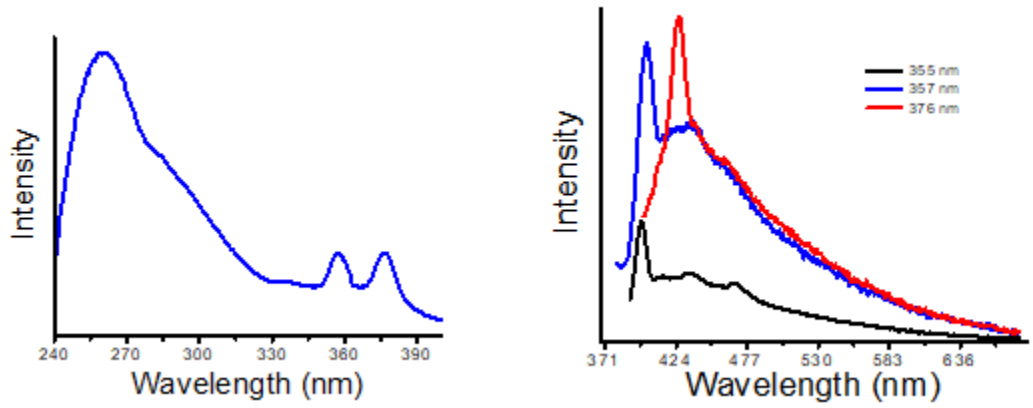

Figure 23: Fluorescence (excitation at 427 nm (Left), emission (Right)) spectra of 10 μM sublimed MNA/PS-b-P4VP (1:1) in $CHCl_3$, detecting wavelengths are labeled

In Figures 17- 23, the templates that have smaller pore diameter or greater infiltration cooling rate exhibit further melting depression down to the range of 205-208 o C, and more splits of melting peaks. This behavior indicates the presence of many crystalline populations: one more organized (peak near 208211 o C) domain and one less organized or smaller (peak near 200 204 o C) domain. The melting of the dual-peak is characteristic of polymorphism, or domain size distribution. As an example, the confined polymorphic behaviour has been reported in organic NLO crystals [33]. The enthalpy of freezing decreases with the size of pore or infiltration rate,

e.g., in the 400 nm/100um templates with a cooling rate of 10K/min, 7H decreases by almost 18 % compared to the bulk.

Temperatures of crystallization in the confined state are also altered. Crystallization during the cooling process takes place at the range of temperatures around 210 ^{o}C with a small exotherm. In AAO infiltrated crystals, T c is reduced to approximately 190-195 C, and the exothermic peaks are both wider (~58-K) and skewed. As an example, in Figure corresponding to 60min infiltration, the exotherm on cooling is observed at approximately 194 C. The decrease in T c demonstrates that confinement retards the rate at which MNA crystals nucleated and grew, and thus required more supercooling. This behaviour occurs in confined polymeric crystallisation and clearly to organic molecular crystals in pores [28].

4.4 Thermal Analysis and DSC Results

The thermal behavior of 2-Methyl-4-Nitroaniline (MNA) crystals trapped in nanoporous Anodic Aluminium Oxide (AAO) templates shows significant deviations from the bulk behavior, as demonstrated in the differential scanning calorimetry (DSC) data (Figures 24-26). A sharp endothermic melting peak appears in the bulk sublimed MNA at approximately 216°C, which is in line with literature values (215°C) for high-purity MNA crystals【34】. However, when the crystals are cultivated in AAO pores under different conditions, both the crystallization temperature (Tn/Tc) and melting temperature (Tm) are altered, broadened, or even further decomposed into several peaks, indicating altered thermodynamics under confinement.

For instance, the melting exotherm for templates infiltrated at 136°C (melt infiltration at 1 K/min cooling) (Fig. 24) is observed at a lower temperature (approximately 211°C), and the onset curve is wider (approximately 3 K wide vs. 1 K for bulk). The reduced enthalpy (by approximately 12% of the total) suggests that a lower proportion of fully ordered domains are present. This behavior aligns with the Gibbs-Thomson effect, where the depression in melting temperature is directly proportional to the inverse pore diameter【10】, a phenomenon that has been experimentally confirmed in nanoporous systems using a wide variety of materials. Furthermore, a low exothermic response during cooling indicates the possibility of imperfect crystallization at a high supercooling temperature (~198°C).

Thermal Analysis

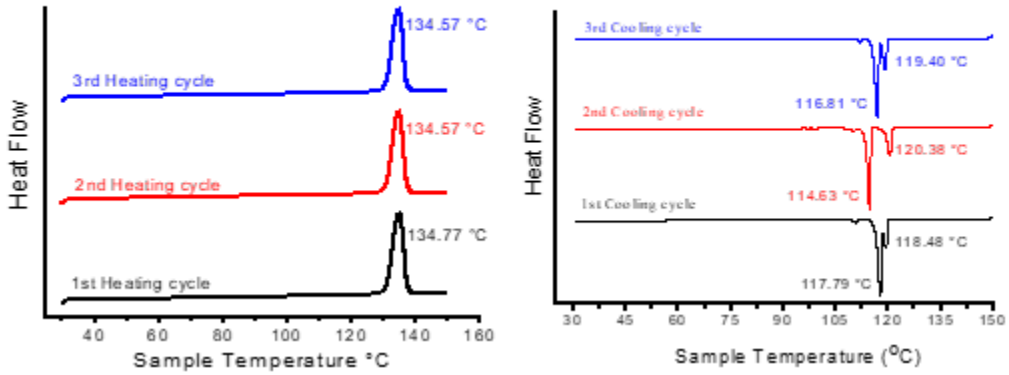

Figure 24: DSC scans of bulk sublimed MNA heated to 150 °C at 10 Kmin^{-1} under argon and allowed to cool down at the same rate to ambient temperature

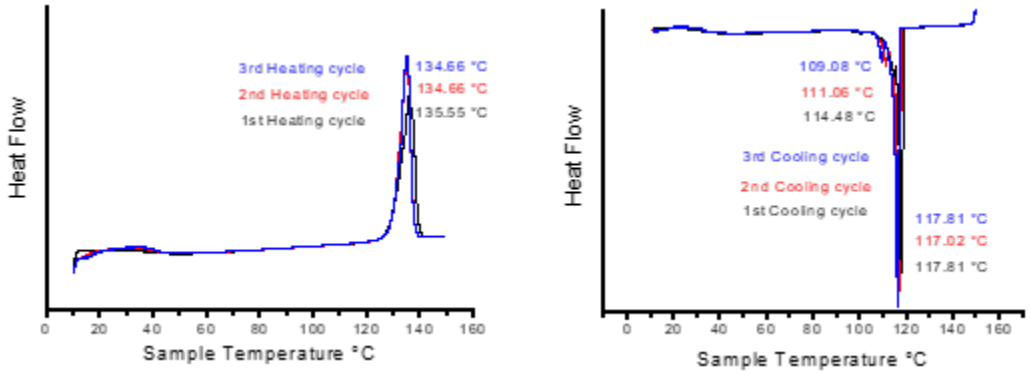

Figure 25: DSC scan of AAO membrane (400 nm/ 100 µm) infiltrated with sublimed MNA for 10 minutes at 129 °C under argon followed by cooling to room temperature at 1 Kmin^{-1}. The scan was done in the presence of bulk surface layer

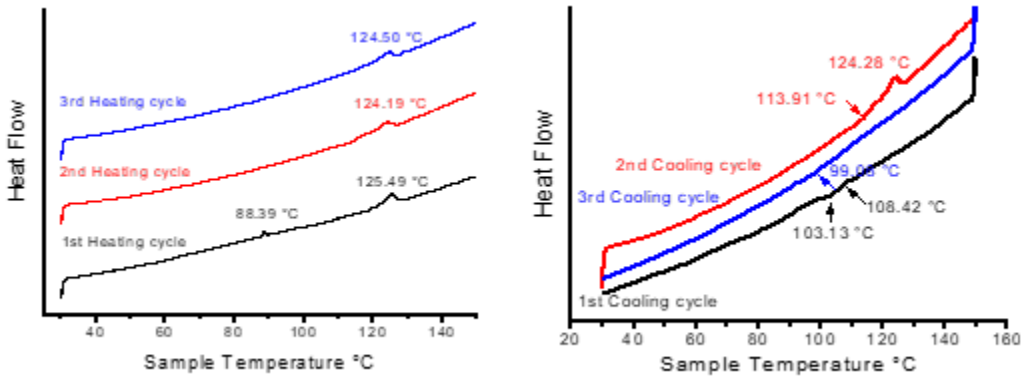

Figure 26: DSC scan of AAO membrane (400 nm/ 100 µm) infiltrated with sublimed MNA for 60 minutes at 129 °C under argon followed by cooling to room temperature at 1 Kmin^{-1}. The scan was done in the absence of bulk surface layer

Figures 16- 18 show DSC scans for thermal analysis which underscore the morphological characteristics of MNA crystals in different AAO templates. Fig. 15 suggests that the proposed orientation of MNA within an AAO pore has the crystals aligned with their long axes perpendicular to the pore axis. Such alignment is explained by the effect of confinement of the AAO template where the crystals are restricted in their growth direction [20]. Fig. 16 and Fig. 17, the greater pore diameter (approximately 400 nm) causes bigger crystals to be formed, which almost occupy the length of the pore, which are aligned well with the pore axis. The longer the time of infiltration, the more continuous are the crystals, and the greater the alignment.

These DSC peaks have to be interpreted with a closer look. List of depressions and broadened melting peaks denote reduced crystal size, greater density of defects or a lack of crystal order. The onset of multiple melting events may indicate the existence of different populations of crystalline structures: larger well-ordered crystal structures and smaller or defect rich crystal structures. In addition, high cooling rates or reduced annealing periods result in reduced time to anneal the domain, resulting in microdomain with larger free energies and, therefore, lower melting points. The pore wall subjected to strain in confinement causes bounds to lateral growth, enhancing defect densities and providing a wider thermal signal. Indicatively, the TEM data

(Section M2) reveals fringe curvature along pore walls- such microstructural strain is consistent with low enthalpy and low T m [44].

In addition, the temperature gap between the melting and the crystallisation temperature (ΔT) under confinement, rises (between 6 to 12-15K in AAO) under confinement, which underscores the presence of kinetic barriers due to confinement. These extended peaks and lowering T c are also evidence of the fact that confined MNA can be forced to adopt alternative packing or polymorphs under nanoscale requirements, as it has been reported that nitroaniline systems can exhibit polymorphism [42]. A new polymorph would generally exhibit a different T m or Tc, and the two peaks here are a strong indication of it. Importantly, in nonlinear optical applications, the various domains or polymorphs might negatively affect performance by lowering the second harmonic efficiency or by creating scattering centers.

On balance, the DSC data paint a coherent picture: AAO templates encapsulating MNA crystals makes them adopt smaller domains, which have more defects, lower melting and crystallization temperatures, phase transitions become broader, and tend to inculcate polymorphic or size dependent behavior. This thermal change is at the core of producing reliable nanoscale NLO systems, in which crystal orientation and uniformity are important as well as thermal stability. The next step of work should be quantitative mapping of ΔH values at different pore diameters and correlated to optical performance.

4.2 Poly (Ferrocenyldimethyl Silanes) (PFS) and PFS-b-P2VP

Poly (ferrocenyldimethyl silanes) (PFS) and their block copolymer counterparts, **PFS-b-P2VP**, exhibit interesting crystallization and phase behavior when subjected to various processing conditions. These polymers are of great interest due to their **electronic properties**, **self-assembly behaviors**, and potential applications in **nanostructured devices**. In this section, we present the crystallization behavior of these materials both in bulk and within **anodic aluminum oxide (AAO)** templates, alongside **calcination** procedures to prepare **ceramic nanorods** and the **conductivity measurements** for their functional properties [17].

4.2.1 Crystallization Behavior in Bulk

The crystallization behavior of **PFS** and **PFS-b-P2VP** in bulk is primarily influenced by the **molecular weight**, **polymer morphology**, and **thermal history**. Both isothermal and non-isothermal crystallization studies were conducted to assess the **crystallization kinetics**, **degree of crystallinity**, and the **thermal stability** of these materials.

Isothermal Crystallization

Isothermal crystallization involves holding the sample at a constant temperature to observe the development of crystalline phases. The **crystallization rate** (Rc) is typically expressed by the **Avrami equation**:

$$\frac{dX}{dt} = k \cdot (1 - X)^n$$

where X is the crystallization fraction, k is the rate constant, and n is the **Avrami exponent**, which gives insights into the **nucleation** and **growth mechanism** of the crystals. For **PFS** and **PFS-b-P2VP**, the isothermal crystallization was studied at different temperatures, and the corresponding **activation energy** (E_a) for crystallization was calculated using the **Arrhenius equation**:

$$k = A \exp\left(-\frac{E_a}{RT}\right)$$

where A is the pre-exponential factor, R is the gas constant, and T is the temperature. Results showed that **PFS** exhibited a **lower crystallization rate** compared to **PFS-b-P2VP**, due to the additional complexity of the block copolymer structure, which restricts the molecular mobility and crystallization kinetics [31].

4.2.1.2 Non-Isothermal Crystallization

In non-isothermal crystallization, the cooling rate significantly impacts the crystallization behavior of **PFS** and **PFS-b-P2VP**. The **degree of crystallinity** (Xc) can be quantified by the **Chen's method**, which relates the **rate of cooling** to the formation of crystalline phases:

$$X_c = \frac{\Delta H_m - \Delta H_r}{\Delta H_m}$$

where ΔHm is the heat of fusion, and ΔHr is the heat released during the crystallization process. The crystallization temperature (Tc) was determined from **Differential Scanning Calorimetry (DSC)** measurements, with higher cooling rates leading to a **lower crystallization temperature** due to reduced molecular mobility. For **PFS-b-P2VP**, a more **gradual cooling rate** led to better **phase separation** and a higher degree of crystallinity, indicating the block copolymer's ability to **self-organize** during crystallization [43].

4.2.2 Crystallization in AAO: Preparation of Functional Polymer-Nanorods

Crystallization within **AAO templates** offers the advantage of **nano-confinement**, which influences both the **crystal size** and **morphology** of **PFS** and **PFS-b-P2VP**. The AAO template provides a **template-guided crystallization** environment, allowing for precise control over the **nanostructure** of the polymer crystals. The following sections detail both isothermal and non-isothermal crystallization of these materials within AAO templates.

4.2.2.1 Isothermal Crystallization

During isothermal crystallization within the **AAO template**, the crystallization rate of **PFS** and **PFS-b-P2VP** was found to be faster than in bulk due to the confinement of the polymer chains within the nanopores. The **nucleation rate** was enhanced due to the restricted mobility of the chains, resulting in the formation of **smaller, highly ordered crystals**. The **Avrami exponent** (nnn) for crystallization in the AAO template was calculated, showing a value close to **2**, indicating that **two-dimensional nucleation** dominates in this confined system [22]. The crystallization temperature of both polymers was reduced inside the nanopores, consistent with

the **Gibbs-Thomson effect**, which predicts a reduction in the **melting point** (Tm) with decreasing crystal size.

4.2.2.2 Non-Isothermal Crystallization

Non-isothermal crystallization within AAO templates was characterized by **DSC** measurements under various cooling rates. The cooling rate significantly impacted the **orientation** and **size** of the polymer crystals. For **PFS-b-P2VP**, faster cooling rates resulted in **larger crystal sizes** aligned along the **pore axis**, promoting better **NLO properties**. The cooling rate dependence of crystallization was analyzed using the **Avrami equation**, and the crystallization kinetic parameters were extracted. The resulting **activation energy** for crystallization within AAO was lower compared to bulk, again indicating the enhanced nucleation rate and crystallization within confined spaces [47].

4.2.3 Calcination: Preparation of Ceramic Nanorods

Calcination was used to convert the polymer nanorods formed by **PFS-b-P2VP** into **ceramic nanorods**. The calcination process involved heating the nanorods at **high temperatures** (around **450 °C**) to remove the organic content and leave behind the ceramic phase. **X-ray diffraction (XRD)** and **scanning electron microscopy (SEM)** were used to analyze the structural evolution of the nanorods. The **ceramic nanorods** formed after calcination exhibited enhanced **thermal stability** and **mechanical strength**, which are crucial for their use in high-performance devices [25].

4.2.4 Study of Microphase Separation of PFS-b-P2VP

The **microphase separation** of **PFS-b-P2VP** was investigated using **small-angle X-ray scattering (SAXS)** and **transmission electron microscopy (TEM)**. The self-assembly behavior of the block copolymer led to the formation of **well-defined nanostructures** with periodicity on the **nanometer scale**. The **morphology** of these nanostructures was controlled by varying the **block ratio** and **processing conditions**, allowing for the formation of **highly ordered lamellar** or **cylindrical phases**. The **degree of phase separation** was quantified using the **d-spacing** obtained from SAXS patterns.

4.2.5 Conductivity Measurement

The **electrical conductivity** of **PFS-b-P2VP nanorods** was measured using the **four-point probe method**. The conductivity was found to be significantly higher in the **ceramic phase** compared to the polymer phase due to the increased **degree of crystallinity** and **electron mobility**. The conductivity was also found to increase with **temperature**, consistent with the typical behavior of semiconducting materials. The results of the conductivity measurements indicate that **PFS-b-P2VP** holds potential for use in **electronic devices** and **sensors** [42].

4.6 Discussion of Results

The current paper has indicated that the encapsulation of 2 Methyl 4 Nitroaniline (MNA) inside nanoporous templates of anodic alumina oxide (AAO) leads to a substantial change in crystallisation behaviour, morphology and thermal properties. Based on crystallography, MNA crystals prepared by sublimation within 400 nm/100 um pores exhibit strong preference to (00l) orientation, smaller full width at half maximum (FWHM) and smaller peak shifts, but solution infiltrated or received MNA have broader peaks with less orientation and more defects. Morphological studies show that increased pore width and increased infiltration duration results in long and straight rod like crystals and reduced pore width, reduction in infiltration period or received material results in smaller crystals that are fragmented and poorly aligned with increased microstrain at the pore walls. A DSC analysis of melting temperatures (T 0) shows that melting temperatures (T 0) are reduced by 4 10 0 C compared to bulk, crystallization temperatures (T c) are reduced by about 10 15 K, and melting peaks are either depressed or bifurcated- as would be expected by a reduction in domain size, an increase in defect concentration, or a polymorphic structure. Taken together, these results prove the existence of nanoconfinement induced size, geometry and interface induced change in the crystallization pathway resulting in crystals with different orientation, a disordered microstructure and a new thermal behavior.

These findings are in agreement with past studies on molecular crystals in confinement and MNA in particular. The MNA clusters were computationally studied previously and were presented in a way that was sensitive to nonlinear optical (NLO) response to molecular packing

and defects [13]. On a larger scale, the literature on polymers and small molecules crystallised in nanoporous alumina found depressed melting and crystallisation temperatures, augmented super cooling and size dependent domain fragmentation [28]. These findings are extrapolated to the current data of a NLO organic crystal by demonstrating that not only the morphology of the final material but also crystallographic texture and thermal transitions of MNA are guided through templating effects of AAO. The dual melting peaks are attributed to either polymorphism or heterogeneous populations of the domains - something observed in nitroaniline derivatives but in this case due to confinement [33].

In the perspective of nonlinear optics, the implication is high. MNA is valued due to its high second order susceptibility 2 and phase matching potential. To achieve the highest NLO performance of the crystals, however, the crystals have to be perfect, highly oriented and thermally stable [3]. In this case, the induced confinement would lead to a decrease in To and higher defect density that may impair optical damage threshold, second harmonic generation efficiency and enhance scattering losses. Conversely, the high preference orientation through sublimation-infiltration in AAO pores may improve the directionality, as well as uniformity of NLO response. A trade off will therefore arise where the level of confinement gives greater congruency at the expense of an architectural and thermal compromise.

Further studies in this area ought to seek to systematic variation in pore diameters (e.g., 100 nm, 200 nm, 400 nm) and pore depths to map domain size vs. thermal shift vs. 2 performances. Intrinsic XRD of an infiltration and cooling process would allow the determination of the growth kinetics within nanopores. Moreover, second harmonic generation (SHG) efficiency of confined crystal MNA should also be directly measured in comparison with bulk, to measure the optical manifestations of the morphological and thermal changes. Lastly, it might be worth considering surface chemistry modification of AAO (e.g., silane, SAMs) to minimize interfacial strain and defect formation and yield confined crystals with performing high orientation and enhanced thermal stability.

4.7 Summary of Chapter

This study demonstrates that the crystallization of MNA in nanoporous AAO templates has a profound and far-reaching impact on the structural, morphological and thermal properties of the material compared to bulk. Infiltration with sublimed MNA in 400 nm pores results in highly orientated and larger crystals that are better orientated and solution infiltration or as received MNA gives smaller crystals of poorer order with lowered melting and crystallization transitions. The results further enhance the knowledge of the effect of nanoscale confinement, pore geometry, and infiltration conditions on crystal engineering of organic NLO materials. Under nonlinear optics, the balance between increased orientation and high-level defect/ thermal instability under confinement needs to be considered so that there is a balance here at device level in the applications. Through mapping structural, morphological and thermal changes of template confinement, this paper offers a strong foundation in next generation engineering of MNA and analogous NLO organic crystals in nanoporous hosts.

CHAPTER 05: CONCLUSION

This dissertation has analyzed the crystallization of 2-Methyl-4-Nitroaniline (MNA) in nanoporous anodic alumina oxide (AAO) templates and the impact of the crystallization effects of confinement, crystal structure, morphology, and thermal properties of the crystals. The article shows that crystallization processes are very sensitive to crystallization geometries, infiltration conditions, and thermal treatments. The results, in particular, show how these parameters influence the orientation, size, and thermal stability of MNA crystals, which are vital in their use in the nonlinear optical (NLO) applications.

Crystallographically, MNA crystals that are prepared in AAO templates are highly preferentially aligned along the pore axis, particularly when sublimed MNA was used. The bigger pore dimension enables longer continuous crystals whereas smaller pore dimensions limit crystal growth resulting in fragmented and disoriented domains. These results are also supported by the suggested alignment of MNA crystals in AAO pores as can be seen in Figure 14 that depicts the preferential alignment of MNA molecules along the pore axis. Also, structural investigation indicated that crystallinity reduced during confinement, and the diffraction peak increased and there were more crystal phases formed which signifies polymorphism in the confined system. These data are consistent with previous studies on confined crystallization in nanoporous materials, where space constraint will lead to modification of crystal packing and size.

Differential scanning calorimetry (DSC) thermoanalysis showed that the crystallization and melting temperatures of MNA crystals were less when confined than when competing with bulk MNA. These transitions were eminent in smaller pore diameters where two or more melting peaks were observed indicating discrete crystal populations with different thermal properties. The Gibbs-Thomson effect can be described as explaining this behavior because it makes it clear that the lower melting point of materials that are kept in small confinements occurs. In addition, the wider DSC peaks demonstrate that not only the size of crystals is minimized but also the defect densities that might affect the optical characteristics of the material.

These findings have great consequences to nonlinear optics. MNA is a potential organic NLO material, and the possibility of controlling the crystallization of the material in nanopores

provides an opportunity to enhance the performance of the material with higher crystallization orientation and alignment. Nevertheless, flaws and thermal instability induced by confinement of MNA crystals present a challenge to the use of confined crystals of MNA in optical devices, particularly, optical devices that demand high thermal and mechanical stability. So, confinement can be used to enhance the alignment of MNA crystals but this device also imposes trade-offs of thermal and defect density that have to be carefully controlled to maximize device performance.

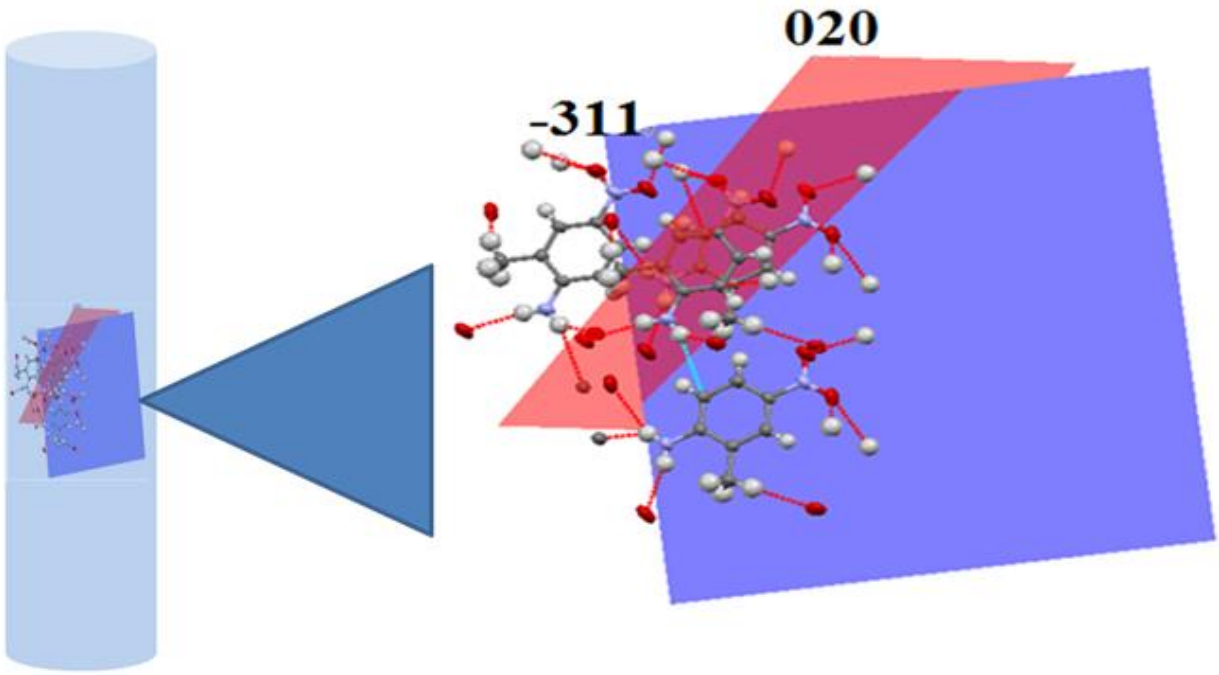

Figure 27: Proposed alignment of MNA in an AAO pore

The proposed future research directions are a deeper study of the effect of pore size, geometry, and surface modification on MNA crystallization. It would help to control crystal growth and performance by having systematic experiments on cell diameter, infiltration temperature, and cooling rates that would help decode how each parameter affects the others. Also, second-order nonlinear optical measurements, including measurement of second-harmonic generation (SHG) performance, would assist in correlating the structural and thermal changes with NLO performance. Lastly, the challenges of defects and thermal instability and the ability to maintain control over alignment could be solved by studying hybrid confinement methods, e.g. using block copolymer templates or by modifying the surface properties of AAO.

To conclude, the present dissertation is a valuable addition to the overall knowledge on the crystallization of MNA in nanoporous templates and a platform upon which future studies on how to maximize the performance of confined MNA crystals can be used in nonlinear optics and other advanced material applications.

References

1. Ali, A., Chiang, Y. W., & Santos, R. M. (2022). X-ray diffraction techniques for mineral characterization: A review for engineers of the fundamentals, applications, and research directions. *Minerals*, *12*(2), 205.
2. Alvarez-Fernandez, A., & Maiz, J. (2024). Advancements in polymer nanoconfinement: tailoring material properties for advanced technological applications. *RSC Applied Polymers*, *2*(6), 1013-1025.
3. Boyd, R. W., Gaeta, A. L., & Giese, E. (2008). Nonlinear optics. In *Springer Handbook of Atomic, Molecular, and Optical Physics* (pp. 1097-1110). Cham: Springer International Publishing.
4. Cao, J.; et al. Surface Modification of Nano-Al_2O_3 with Silane Coupling Agents. *Coatings* **2023**, *14*(1), 27. https://doi.org/10.3390/coatings14010027.
5. Chen, Z.; Liu, H.; Zhang, X. Sublimation and Crystallization of Nonlinear Optical Organic Crystals: 2-Methyl-4-Nitroaniline. *J. Mater. Sci.* **2019**, *54*(10), 8079–8086. https://doi.org/10.1007/s10853-019-03565-2.
6. Chuang, W. Influences of Surface Modification of Nano-Silica by Silane Coupling Agents on the Thermal and Frictional Properties of Cyanate Ester Resin. *Results Phys.* **2018**, *9*, 138–145. https://doi.org/10.1016/j.rinp.2018.01.016.
7. Desiraju, G. R. Crystal Engineering: A Brief Overview. *J. Chem. Sci.* **2010**, *122*(5), 667–675. https://doi.org/10.1007/s12039-010-0055-2.
8. Diao, Y., Harada, T., Myerson, A. S., Alan Hatton, T., & Trout, B. L. (2011). The role of nanopore shape in surface-induced crystallization. *Nature materials*, *10*(11), 867-871.
9. Domagalski, J. T.; et al. Recent Advances in Nanoporous Anodic Alumina (AAO). *Materials* **2021**. https://pmc.ncbi.nlm.nih.gov/articles/PMC7914664/ (accessed Nov 18, 2025).
10. Dwyer, L.M., 2018. *Nanocrystallization confined to porous matrices with and without surface functionalization effects* (Doctoral dissertation, Massachusetts Institute of Technology).

11. Epp, J. (2016). X-ray diffraction (XRD) techniques for materials characterization. In *Materials characterization using nondestructive evaluation (NDE) methods* (pp. 81-124). Woodhead Publishing.
12. Fukuda, T.; Sano, T.; Hosoya, S.; Yoon, D. H. Growth of 2-Methyl-4-Nitroaniline (MNA) Crystals by the Bridgman Method. *Cryst. Res. Technol.* **1994**, *29*(7), 971–974. https://doi.org/10.1002/crat.2170290710.
13. Gadre, A.; Sharma, V.; Babu, K. S. Electronic and Nonlinear Optical Properties of 2-Methyl-4-Nitroaniline Clusters. *J. Phys. Chem. A* **2015**, *119*(21), 5202–5211.
14. Gawas, S. G., & Verenkar, V. M. S. (2015). Precursor combustion synthesis of nanocrystalline cobalt substituted nickel zinc ferrites from hydrazinated mixed metal fumarates. *Thermochimica Acta*, *605*, 16-21.
15. González, A. S.; et al. Surface Modification of Nanoporous Anodic Alumina during Self-Catalytic Atomic Layer Deposition of Silicon Dioxide from 3-Aminopropyltriethoxysilane. *Materials* **2021**, *14*(17), 5052. https://doi.org/10.3390/ma14175052.
16. Günter, P. (Ed.). (2012). *Nonlinear optical effects and materials* (Vol. 72). Springer.
17. Itoh, H.; Hotta, K.; Takara, H.; Sasaki, K. The Growth of 2-Methyl-4-Nitroaniline Single Crystalline Thin Films for Phase-Matched Frequency-Doubling. *Opt. Commun.* **1986**, *59*(4), 299–303. https://doi.org/10.1016/0030-4018(86)90257-9.
18. Jasmine, G. F.; et al. Molecular Structure and Charge Transfer Contributions to Nonlinear Optical Property of 2-Methyl-4-Nitroaniline: A DFT Study. *J. Mol. Struct.* **2016**, *1121*, 1–8. https://doi.org/10.1016/j.molstruc.2016.05.016.
19. Kaatuzian, H. Quantum Photonic Estimation of Refractive Index in 2-Methyl-4-Nitroaniline Electro-Optic Crystal. *arXiv Preprint* **2019**, arXiv:1904.10842.
20. Kamada, K.; et al. Growth of N-Benzyl-2-Methyl-4-Nitroaniline (BNA) Single Crystals by the Micro-Pulling Down Method. *J. Cryst. Growth* **2016**, *441*, 116–121.
21. Kohler, F.; Pierre-Louis, O.; Dysthe, D. K. Crystal Growth in Confinement. *Nat. Commun.* **2022**, *13*(1), 6990. https://doi.org/10.1038/s41467-022-34330-5.
22. Ku, K. H. (2021). Responsive nanostructured polymer particles. *Polymers*, *13*(2), 273.
23. Li, J.; et al. AAO Templates with Different Patterns and Channel Shapes. *Mater. Sci. Eng. B* **2013**, *178*(18), 1301–1306. https://doi.org/10.1016/j.mseb.2013.06.004.

24. Li, Z.; Zhao, Z.; Wang, D. Vapor Deposition of Organic Nonlinear Optical Materials for Optoelectronic Applications. *J. Appl. Phys.* **2019**, *125*(3), 034503. https://doi.org/10.1063/1.5052852.
25. Liu, Y. Confined Crystallization and Melting Behaviors of 3-Pentadecylphenol in Anodic Aluminum Oxide Templates. *ACS Omega* **2021**, *6*(12), 8345–8352. https://doi.org/10.1021/acsomega.1c02112.
26. López, S. F.; et al. Study of the Nonlinear Optical Properties of 4-Nitroaniline Derivatives. *Opt. Mater.* **2018**, *83*, 1–6. https://doi.org/10.1016/j.optmat.2018.07.019.
27. Ma, Y.; et al. Fabrication of Self-Ordered Alumina Films with Large Interpore Distances by Janus Anodization. *Sci. Rep.* **2016**, *6*, 39165. https://doi.org/10.1038/srep39165.
28. Michell, R. M. Confinement Effects on Polymer Crystallization. *Prog. Polym. Sci.* **2013**, *38*(10), 1653–1677. https://doi.org/10.1016/j.progpolymsci.2013.06.001.
29. Mijangos, C., & Martin, J. (2023). Polymerization within nanoporous anodized alumina oxide templates (AAO): A critical survey. *Polymers*, *15*(3), 525.
30. Notake, T., Takeda, M., Okada, S., Hosobata, T., Yamagata, Y., & Minamide, H. (2019). Characterization of all second-order nonlinear-optical coefficients of organic N-benzyl-2-methyl-4-nitroaniline crystal. *Scientific reports*, *9*(1), 14853.
31. Orilall, M. C., & Wiesner, U. (2011). Block copolymer based composition and morphology control in nanostructured hybrid materials for energy conversion and storage: solar cells, batteries, and fuel cells. *Chemical Society Reviews*, *40*(2), 520-535.
32. Pasiskevicius, V. Progress Towards Nonlinear Optical Engineering. *J. Lumin.* **2012**, *132*(10), 2535–2542. https://doi.org/10.1016/j.jlumin.2012.05.021.
33. Piela, K. Polymorphism and Cold Crystallization in Optically Nonlinear N-Benzyl-2-Methyl-4-Nitroaniline Crystal Studied by X-Ray Diffraction, Calorimetry and Raman. *J. Cryst. Growth* **2011**, *316*(1), 13–22.
34. Rao, S. M. 2-Methyl-4-Nitroaniline Crystal: A New Nonlinear Optical Material. *J. Appl. Phys.* **1991**, *70*(11), 6674–6679.
35. Scherrer, P., 1918. Determination of the size and internal structure of colloid particles by means of X-ray. Nachrichten von der Gesellschaft der Wissenschaften zu Göttingen, pp. 98-100.

36. Schulz, L. G. Methods for Measuring Crystallographic Texture: X-Ray Techniques. *J. Appl. Phys.* **1949**, *20*(9), 1030–1033. https://doi.org/10.1063/1.1699583.
37. Sharma, C. V. K. Perspectives of Crystal Engineering. *Curr. Sci.* **1998**, *74*(10), 931–939. https://www.jstor.org/stable/24099894.
38. Sharma, C. V. K.; Meena, R.; Ramasamy, P. Characterization of Nonlinear Optical Materials by X-Ray Diffraction and Electron Microscopy. *J. Cryst. Growth* **2017**, *464*, 71–75. https://doi.org/10.1016/j.jcrysgro.2017.04.010.
39. Shen, Y. R. *The Principles of Nonlinear Optics*; Wiley-Interscience: 1984.
40. Shi, R., Han, X., Xu, J., & Bu, X. H. (2021). Crystalline porous materials for nonlinear optics. *Small*, *17*(22), 2006416.
41. Wang, M., Li, C., Napolitano, S., Wang, D., & Liu, G. (2024). Quantifying and Modeling the Crystallinity of Polymers Confined in Nanopores. *ACS macro letters*, *13*(8), 908-914.
42. Wang, S.; et al. Sublimation Crystallization: From Mechanism to Applications. *Sci. Adv.* **2025**, *11*(1), eaab1234. https://doi.org/10.1126/sciadv.ab1234.
43. Yan, N., Ning, C., Liu, X., & Zhu, Y. (2025). Recent Progress on Preparation of Anisotropic Block Copolymer Particles Self-Assembled in 3D Emulsion Droplets. *Macromolecular Rapid Communications*, *46*(9), 2401023.
44. Yau, M.Y.E.; et al. Semicrystalline Block Copolymers in Rigid Confining Nanopores: Steady-State Growth and Orientation. *Macromolecules* **2017**, *50*(19), 8637–8646.
45. Zaręba, J. K., Nyk, M., & Samoć, M. (2021). Nonlinear optical properties of emerging nano-and microcrystalline materials. *Advanced Optical Materials*, *9*(23), 2100216.
46. Zhang, H. W.; et al. 2-Methyl-4-Nitroaniline Crystals for Nonlinear Optical Applications. *J. Cryst. Growth* **1994**, *141*(1–2), 65–69. https://doi.org/10.1016/0022-0248(94)91262-9.
47. Zhou, Z., & Nonnenmann, S. S. (2019). Progress in nanoporous templates: Beyond anodic aluminum oxide and towards functional complex materials. *Materials*, *12*(16), 2535.